

Aalto University
School of Science
Degree Programme in Engineering Physics

TONY SAVANDER

Thermoelectric effects in hybrid superconducting junctions

Master's Thesis
Espoo, November 26, 2019

Supervisor: Professor Christian Flindt, Aalto University
Advisor: Dr. Pablo Buset, Aalto University

Author:	TONY SAVANDER	
Title:	Thermoelectric effects in hybrid superconducting junctions	
Date:	November 26, 2019	Pages: 43
Major:	Engineering Physics	Code: SCI3056
Supervisor:	Professor Christian Flindt	
Advisor:	Dr. Pablo Bureset	
<p>Traditionally, the view on thermoelectric effects in superconductors has been that if they exist, they must be very weak, as the particle-hole symmetry is fulfilled in most superconductors. However, superconductors contain ingredients for strong thermoelectric effects, because the latter typically require a strong energy dependent density of states, which can be provided by the density of states of a superconductor.</p> <p>If one can break the particle-hole symmetry of the transport processes via some mechanism, superconductors can become very strong thermoelectrics. In superconductors, breaking of the electron-hole symmetry can be achieved with spin polarizing and splitting magnetic fields. This breaks the electron-hole symmetry between the different spin channels, but the global electron-hole symmetry is still maintained.</p> <p>In this work, we study thermoelectric effects in ferromagnet-superconductor hybrid junctions, focusing on the thermoelectric current created by a temperature gradient. The main objective is to verify the necessary conditions in order to have a thermoelectric effect. Another main objective is to determine the effect of the symmetry of the superconducting pairing potential on the thermoelectric current.</p>		
Keywords:	Andreev Reflection, Unconventional Superconductivity, Ferromagnetism, Quantum Transport	
Language:	English	

Acknowledgements

The research included in this thesis was carried out in the Quantum Transport group of the Department of Applied Physics at Aalto University. The thesis work was carried out from June to November 2019.

I would like to thank my supervisor Professor Christian Flindt for the opportunity to work as a member of his group for the past two and a half years as a research assistant. I thank Dr. Pablo Buset for being my instructor. His patience on answering my question and providing ideas and guidance was essential for the completion of this project. I also thank other QTs for discussions and team spirit. I would especially like to single out Elina Potanina for like-minded discussions. Also, Dr. Michael Moskalets visited our group multiple times during my stay, and I wish to thank him for discussions on all topics imaginable. I enjoyed a lot our coffee making sessions with Misha and Pablo. Also thanks to all my office mates along the years, especially Geet Raju for fun discussions on various topics. Also thanks to Antti Karjalainen for coffee comradery.

Thanks to my fellow students Toni Mäkelä and Ville pyykkönen for discussions, long nights of calculating and jazz excursions, which I hope will continue.

I would also like to express my gratitude to University Lecturers Dr. Jami Kinnunen and Dr. Ville Havu, who let me act as a teaching assistant in their courses for almost 5 years. I had many useful discussions with both of them over the years.

Finally, thanks to my family and friends.

Helsinki, November 26, 2019

Tony Savander

Contents

Abstract	2
1 Introduction	5
2 Andreev Reflection	8
3 Theory and methods	10
3.1 Bogoliubov-de Gennes equations	10
3.2 Quasi-one dimensional limit	10
3.3 Pairing potential	11
3.4 Decoupling of spin channels	12
3.5 Singlet-triplet mix	13
3.6 Model for ferromagnet-supeconductor hybrid junctions	14
4 Results	21
4.1 N-I-S junction	21
4.2 Ferromagnet-Superconductor hybrid junctions	25
4.2.1 Temperature effects	31
4.3 Singlet-triplet mix in F-S junctions	32
5 Conclusions	39

Chapter 1 Introduction

Superconductors are materials wherein electrical resistance vanishes and magnetic fields are expelled, below a critical temperature. BCS (Bardeen, Cooper, Schrieffer) theory [1] states that when temperature becomes low enough, attractive interactions between the electrons due to their coupling to the lattice phonons can overcome their repulsive Coulomb interaction and lead to the formation of coherent quantum states of coupled electrons, which are called Cooper pairs [2]. This interaction occurs between electrons with opposite momenta and spins, thus forming a singlet *s*-wave pairing state. Because a certain energy is needed to break these pairs, an energy gap is opened in the electron density of states in the superconductor (SC). In BCS theory, the width of the gap is defined by a material dependent parameter Δ , which is the energy per electron required to break one Cooper pair. Until the discovery of high temperature superconductivity in 1986 [3], it was believed that BCS theory forbade superconductivity above 30K. This reopened the question of the origin of the Cooper pairing, which remains still unanswered.

Many properties of a SC are determined by its pairing potential or the energy gap function. In BCS theory [1] the SC energy gap is isotropic, a conventional singlet *s*-wave pairing. The majority of superconductors feature this pair potential. Currently, all superconductors for which the Cooper pairing cannot be explained by the phonon exchange of BCS-theory but by some other mechanism are referred to as unconventional superconductors [4]. This includes, for example, heavy-fermion superconductors and high critical temperature cuprates. Unlike the conventional *s*-wave superconductors, unconventional superconductors adopt different pairing states, both singlet and triplet. High temperature superconductors could be in a singlet *d*-wave pairing state, which has an internal phase of the pair potential. This has a large influence on the electric properties of the material [5]. Some superconductors, like Sr_2RuO_4 or UPt_3 are believed to have a triplet pairing potential [4]. Recently, triplet chiral *p*-wave superconductors have been proposed to host Majorana bound states. Majorana fermions are their own antiparticle, which might provide new possible applications in quantum computing [6].

One of the most interesting consequences of the unconventional pairing is the formation of gapless surface Andreev states (SAS) and the related emer-

gence of a zero bias peak in the tunneling conductance. Superconductors in two dimensions can be classified into two groups, depending on the shape of the energy gap in reciprocal (energy-momentum) space [7]. The first group are the gapful superconductors, where the energy gap is finite and isotropic. An example of this is the conventional BCS s -wave superconductor. The second group are the nodal superconductors, where the energy gap vanishes for certain directions of the momentum. An example of this are the d -wave superconductors. We can also make another classification, depending on whether SAS appear or not, to non-trivial and trivial superconductors, respectively. The BCS s -wave pairing would thus be classified as a trivial gapful, as it has no subgap states. An example of non-trivial nodal superconductor would be the p_x -wave pairing, for which the surface states result in a zero bias peak in the tunneling conductance. The tunneling normal metal(N)-barrier(I)-superconductor(S) (N-I-S) junction can be used to study the SAS and other properties of unconventional superconductors [5].

Thermoelectric effects, electric potentials created by temperature gradients, are currently intensively studied because of their possible use in converting waste heat from various processes to useful energy. In electronic conductors the requirement for thermoelectricity is breaking of the symmetry between positive- and negative-energy charge carries, particles and holes, respectively [8]. If they exist, thermoelectric effects in superconductors must be very weak, since the particle-hole symmetry is fulfilled in most superconductors. However, thermoelectric effects in superconductors could be potentially very large, due to the strong energy dependent density of states of the superconductor. Breaking of the particle-hole symmetry can be achieved by combining superconductors and magnetic materials in hybrid junctions. The interplay between superconductivity and magnetism breaks the particle-hole symmetry between the different spin channels, but maintains it globally [9].

In this work, we study thermoelectric effects in ferromagnet-superconductor (F-S) hybrid junctions, focusing on the thermoelectric current created by a temperature gradient. The main objective is to verify the necessary conditions in order to have a thermoelectric effect. Another main objective is to determine the effect of the symmetry of the pairing potential of the superconductor on the thermoelectric current.

We will employ a scattering theory based on Bogoliubov-de Gennes formalism. The calculation of the conductance and the current is determined by the transmission and reflection amplitudes between different channels at the interfaces of the studied heterostructure. Scattering formalism based on the

Bogoliubov-de Gennes equations has been adapted by Blonder et al. (BTK formalism) to one-dimensional N-I-S junction with a BCS superconductor [10]. BTK formalism was further generalized to include anisotropic superconductors by, among others, Kashiwaya and Tanaka [11][12][5]. The BTK theory was then generalized to describe ferromagnetic-insulator-superconductor (F-I-S) junction in one dimension with a BCS superconductors by de Jong and Beenakker [13] and this was further extended to ferromagnet-ferromagnetic insulator-superconductor (F-FI-S) junction with anisotropic d -wave pairing by Kashiwaya et al. [14].

This thesis is organized as follows. In Chapter 2, we will explain the process of Andreev reflection. In Chapter 3 we will introduce the Bogoliubov-de Gennes formalism and describe our model for F-S junctions. In Chapter 4 we will present our results. First we will discuss the properties of different types of pairing symmetries for the N-I-S junction. We also discuss a pairing symmetry that mixes singlet and triplet type pairings. Then, we will study the F-FI-S junction in detail with different pairing symmetries, including the singlet-triplet mix. In Chapter 5 we summarize our findings and provide some outlook for the future.

Chapter 2 Andreev Reflection

Andreev reflection is a microscopic scattering process taking place at the interface of a normal metal- superconductor (N-S) junction, by which normal current in the normal metal is converted to a supercurrent in the superconductor. Andreev reflection was first proposed by Andreev when studying heat transport at N-S interfaces [15]. Consider a clean N-S interface as sketched in figure 2.1. An electron in the normal metal is incoming to the interface with wave vector \mathbf{k} and excitation energy ε measured from the Fermi energy E_F such that it is smaller than the superconducting energy gap Δ . Since the superconductor has a gap in the density of states, the electron cannot propagate into the superconductor. The only scattering process that can take place is an Andreev reflection. The incoming electron couples with another electron in the normal metal with opposite wave vector $-\mathbf{k}$ and energy $-\varepsilon$ and forms a Cooper pair in the superconductor, transferring charge $2e$ into the superconductor. The empty state below the Fermi energy left behind by this electron is reflected back into the normal metal as a hole. The reflected hole has an opposite charge with respect to the incident electron.

Most common superconductors have Fermi energies E_F much larger than the superconducting energy gap Δ . Thus, if we neglect terms of the order Δ/E_F , both the incident electron and the reflected hole have the same wave vector \mathbf{k} . While the velocity of the incident electron is parallel to its wave vector, the velocity of the reflected hole is opposite to it and the hole is retroreflected. It can be said that the reflected hole traces back the path of the incident electron. This process regulates the conversion of the dissipative normal current in the normal metal into supercurrent in the superconductor and has a positive sign for the local conductance. Time reversal of this process is the conversion of supercurrent into normal current, where the incoming hole is filled by an electron constituting a Cooper pair and the other electron moves away in the normal region.

The retroreflected hole contains interesting properties in relation to the incident electron. First, it has an opposite charge. Second, at Fermi energy E_F , the dynamical phase of the hole is conjugated. Also, the hole acquires an additional phase shift due to the macroscopic phase of the superconductor. This has a great impact in the conductance of Josephson junctions, where

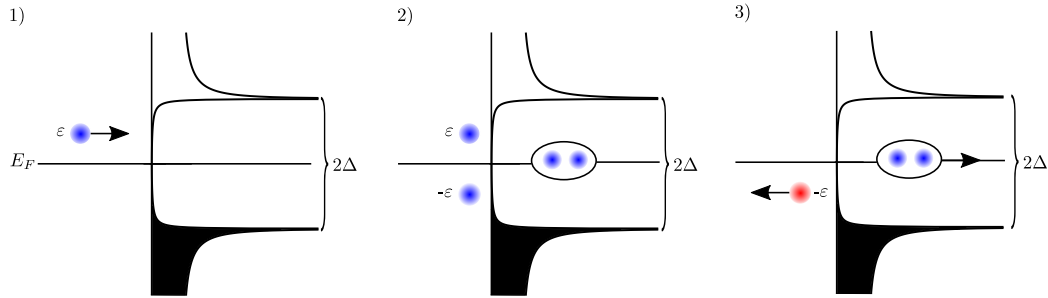


Figure 2.1: Andreev reflection 1) An electron in the normal metal is incoming to the interface with wave vector \mathbf{k} and excitation energy $\varepsilon < \Delta$ 2) The incoming electron couples with another electron in normal metal with opposite wave vector $-\mathbf{k}$ and energy $-\varepsilon$ and forms a Cooper pair 3) Charge $2e$ is transferred into the superconductor while the empty state below the Fermi is reflected back as a hole.

an oscillation of the conductance with the phase difference between SCs can be observed. Finally, depending on the pairing potential, the retroreflected hole can have an opposite spin, which is the case for most superconductors.

The existence of Andreev reflection may actually be considered as microscopic mechanism to explain the proximity effect in the normal metal. The amplitude of the Andreev reflection is proportional to the pairing amplitude at the N-S interface [16].

Consider now a normal metal-superconductor junction with an insulating barrier at the interface (N-I-S). In the tunneling limit, when the insulating barrier is strong, the conductance spectrum is directly proportional to the density of states of the superconductor and we can study the surface states of unconventional pairings. In the presence of a surface state there is a perfect Andreev reflection in the tunneling limit. In the absence of surface state an incoming electron is normally reflected back from the interface. We will discuss the conductance spectrum for different pairing potentials in the N-I-S junction in section 4.1 in detail.

Chapter 3 Theory and methods

3.1 Bogoliubov-de Gennes equations

The Bogoliubov-de Gennes (BdG) equations describe the quasiparticle states in superconductors with spatially varying pair potential. As there is a spin dependence on the pairing potential, the BdG-equations can be presented in momentum space by the Nambu (particle-hole)-spin matrix [4]

$$\begin{pmatrix} \hat{H}_0(\mathbf{k}) - E_F \hat{\sigma}_0 & \hat{\Delta}(\mathbf{k}) e^{i\phi} \\ \hat{\Delta}^\dagger(\mathbf{k}) e^{-i\phi} & -\hat{H}_0(-\mathbf{k}) + E_F \hat{\sigma}_0 \end{pmatrix} \Psi(\mathbf{k}) = \varepsilon \Psi(\mathbf{k}), \quad (3.1)$$

where \hat{H}_0 is the single particle Hamiltonian in spin space, E_F is the Fermi energy, $\hat{\sigma}_0$ is the unit matrix in spin space, $\hat{\Delta}(\mathbf{k})$ is the pairing potential matrix in spin space, \mathbf{k} is the wave vector and ε is the energy measured from the Fermi level E_F . ϕ is the superconducting phase, which we can omit due to considering only junctions with one superconductor. The quasiparticle states are expressed in Nambu-spin space by the four-component wavefunction

$$\Psi(\mathbf{k}) = [u_\uparrow(\mathbf{k}), u_\downarrow(\mathbf{k}), v_\uparrow(\mathbf{k}), v_\downarrow(\mathbf{k})]^T, \quad (3.2)$$

where $u_\sigma(\mathbf{k})$ and $v_\sigma(\mathbf{k})$ are the electron and hole-like components with spin $\sigma = \uparrow, \downarrow$.

3.2 Quasi-one dimensional limit

In the following, we consider two-dimensional junctions with smooth interfaces in the quasi-one dimensional limit, where transport takes place along the x-direction and the transverse component of the wave vector k_y is conserved. We can thus parametrize the conserved transverse part of the momentum by using the angle of incidence $\theta = \sin^{-1}(k_y/k_F)$, with the k_F is the Fermi wave vector. We work in the weak-coupling limit, where we assume that the superconducting pairing occurs near the Fermi surface. Then $\hat{\Delta}(\mathbf{k})$ is evaluated at $|\mathbf{k}| = k_F$ and it only has an angular dependence [17]. In unconventional superconductors quasiparticles may experience different effective pair potentials depending on the direction of their momentum. Assuming the band energy ε is the same for left- and right-movers, the sign change related to

the direction of motion is accounted for by the transformation $\theta \rightarrow \pi - \theta$. Thus, for right movers we have pair potential $\Delta(\theta_+)$, with $\theta_+ = \theta$ and for left movers $\Delta(\theta_-)$, with $\theta_- = \pi - \theta$.

3.3 Pairing potential

The spin and momentum structure of the Cooper pairs is encoded in the superconducting gap function, which plays the role of the superconducting order parameter and is directly related to the pair wave function. In the singlet state the pairing is described by a scalar complex function $\Delta_s(\mathbf{k})$. For the conventional s-wave superconductor this function is constant, i.e., $\Delta_s(\mathbf{k}) = \Delta_0$. For the triplet state there are three possible values of the spin projection and therefore the gap function has three complex components, which are parametrized by the spin wave vector $\mathbf{d}(\mathbf{k})$. Cooper pairs are formed by two electrons with the pairing potential $\hat{\Delta}(\mathbf{k}) \sim \langle \psi_{\mathbf{k}_1}^\dagger \psi_{-\mathbf{k}_2}^\dagger \rangle$. Due to Fermi-Dirac statistics the gap function must be anti-symmetric, $\hat{\Delta}(\mathbf{k}) = -\hat{\Delta}^T(-\mathbf{k})$. The spin singlet state is antisymmetric under the exchange of up and down spins, from which it follows that $\Delta_s(\mathbf{k})$ must be even. The triplet is symmetric under spin exchange, and thus $\mathbf{d}(\mathbf{k})$ is odd. A general form of the pairing potential is [4]

$$\begin{aligned} \hat{\Delta}(\mathbf{k}) &= [\Delta_s(\mathbf{k})\hat{\sigma}_0 + \sum_{j=1}^3 d_j(\mathbf{k})\hat{\sigma}_j] i\hat{\sigma}_2 \\ &= \begin{pmatrix} id_2(\mathbf{k}) - d_1(\mathbf{k}) & d_3(\mathbf{k}) + \Delta_s(\mathbf{k}) \\ d_3(\mathbf{k}) - \Delta_s(\mathbf{k}) & id_2(\mathbf{k}) + d_1(\mathbf{k}) \end{pmatrix}, \end{aligned} \quad (3.3)$$

where $\hat{\sigma}_{1,2,3}$ are Pauli matrices in spin space. We consider only the following cases: 1) singlet state $\Delta_s \neq 0, \mathbf{d} = 0$ and triplet states 2) $d_3 \neq 0, \Delta_s = d_1 = d_2 = 0$. For these states the pairing potential matrix is either fully diagonal or anti-diagonal. Table 3.1 shows pairing matrices for different spin states and the corresponding spin channels.

Table 3.1: Pairing matrices and phase factors for different pairing states and spin channels. S (T) stands for singlet (triplet). The phase factor is defined as $\eta_\sigma(\theta) = \Delta_\sigma(\theta)/|\Delta_\sigma(\theta)|$.

Spin state	Pairing matrix	Spin channel	Phase $\eta(\theta)$
S s -wave	$i\Delta_0\hat{\sigma}_2$	$\uparrow\downarrow$	1
		$\downarrow\uparrow$	-1
S chiral d -wave	$i\Delta_0e^{2i\theta}\hat{\sigma}_2$	$\uparrow\downarrow$	$e^{2i\theta}$
		$\downarrow\uparrow$	$-e^{2i\theta}$
S $d_{x^2-y^2}$ -wave	$i\Delta_0\cos(2\theta)\hat{\sigma}_2$	$\uparrow\downarrow$	$\text{sgn}[\cos(2\theta)]$
		$\downarrow\uparrow$	$-\text{sgn}[\cos(2\theta)]$
S d_{xy} -wave	$i\Delta_0\sin(2\theta)\hat{\sigma}_2$	$\uparrow\downarrow$	$\text{sgn}[\sin(2\theta)]$
		$\downarrow\uparrow$	$-\text{sgn}[\sin(2\theta)]$
T chiral p-wave	$i\Delta_0e^{i\theta}\hat{\sigma}_2$	$\uparrow\downarrow$	$e^{i\theta}$
		$\downarrow\uparrow$	$e^{i\theta}$
T p_x -wave	$i\Delta_0\cos(\theta)\hat{\sigma}_2$	$\uparrow\downarrow$	$\text{sgn}[\cos(\theta)]$
		$\downarrow\uparrow$	$\text{sgn}[\cos(\theta)]$
S+T	$(\Delta_s\hat{\sigma}_0 + \Delta_pe^{i\theta}\hat{\sigma}_3)i\hat{\sigma}_2$	$\uparrow\downarrow$	$(\Delta_s + \Delta_pe^{i\theta})/\Delta_1$
		$\downarrow\uparrow$	$-(\Delta_s - \Delta_pe^{i\theta})/\Delta_2$

3.4 Decoupling of spin channels

In all the cases of table 3.1, the pairing potential matrix is either fully diagonal or anti-diagonal. This leads to decoupling of the 4x4 BdG-equations into two spin channels, i.e, two 2x2 equations of the form

$$\begin{pmatrix} H_0 - E_F & s_\sigma\Delta_\sigma(\theta) \\ s_\sigma\Delta_\sigma^*(\theta) & -H_0 + E_F \end{pmatrix} \begin{pmatrix} u_\sigma \\ v_\sigma \end{pmatrix} = \varepsilon \begin{pmatrix} u_\sigma \\ v_\sigma \end{pmatrix}, \quad (3.4)$$

where σ denotes the spin channel, $s_\sigma = (-1)^{\sigma-1}$ for singlet pairings and $s_\sigma = 1$ for triplet pairings. $H_0 = \frac{\hbar}{2m}(\partial_x^2 - k_y^2)$ is the single-particle Hamiltonian in the quasi-one dimensional limit. The general solution can be written as

$$\begin{aligned} \Psi(x, y) &= \Psi(x)e^{ik_y y} \\ &= e^{ik_y y} \left[a_e \begin{pmatrix} u_\sigma(\theta_+) \\ \eta_\sigma^*(\theta_+)v_\sigma(\theta_+) \end{pmatrix} e^{iq_e \cos \theta x} + b_e \begin{pmatrix} u_\sigma(\theta_-) \\ \eta_\sigma^*(\theta_-)v_\sigma(\theta_-) \end{pmatrix} e^{-iq_e \cos \theta x} \right. \\ &\quad \left. + a_h \begin{pmatrix} \eta_\sigma(\theta_-)v_\sigma(\theta_-) \\ u_\sigma(\theta_-) \end{pmatrix} e^{-iq_h \cos \theta x} + b_h \begin{pmatrix} \eta_\sigma(\theta_+)v_\sigma(\theta_+) \\ u_\sigma(\theta_+) \end{pmatrix} e^{+iq_h \cos \theta x} \right], \end{aligned} \quad (3.5)$$

where

$$\begin{aligned}
u_\sigma(\theta) &= \frac{1}{\sqrt{2}} \left(1 + \frac{\sqrt{E^2 - |\Delta_\sigma(\theta)|^2}}{E} \right)^{1/2}, \\
v_\sigma(\theta) &= \frac{1}{\sqrt{2}} \left(1 - \frac{\sqrt{E^2 - |\Delta_\sigma(\theta)|^2}}{E} \right)^{1/2}
\end{aligned} \tag{3.6}$$

are the BCS coherence factors and $\eta_\sigma(\theta) = s_\sigma \Delta_\sigma(\theta) / |\Delta_\sigma(\theta)|$ is the gap phase. Table 3.1 collects gap phases for different pairing states for corresponding decoupled spin channels. The wave vector $q_{e(h)}$ can be written as

$$q_{e(h)} = k_F \sqrt{1 \pm \frac{\sqrt{E^2 - |\Delta|^2}}{E_F}}, \tag{3.7}$$

where the positive (negative) sign is for electron-like (hole-like) quasiparticles. a_e and b_e are the amplitudes for right- and left-moving electron like quasiparticles and a_h and b_h are for right- and left-moving hole-like quasiparticles. One should notice that the actual direction of propagation, i.e. group velocity, for hole-like quasiparticles is opposite to the direction of the momentum. As we are considering transport in the quasi-one dimensional limit, the momentum in the y-direction is conserved and we will omit the y-part altogether from now on. When $\Delta = 0$, the BdG-equations are reduced to the regular Schrödinger equations. General solutions for electrons and holes in the normal metal are

$$\Psi_e(x) = e^{\pm i k_e \cos \theta x} \begin{pmatrix} 1 \\ 0 \end{pmatrix}, \Psi_h(x) = e^{\mp i k_h \cos \theta x} \begin{pmatrix} 0 \\ 1 \end{pmatrix}, \tag{3.8}$$

with

$$k_{e(h)} = k_F \sqrt{1 \pm E/E_F}, \tag{3.9}$$

where the sign in the square root is positive for electrons, negative for holes.

3.5 Singlet-triplet mix

We also consider a general pairing potential that is a mixture of spin-singlet and spin-triplet states. Systems where the Cooper pairs have this type of pairing include non-centrosymmetric superconductors and surface states of topological insulators [18]. Here we assume that the singlet-triplet mix is

that of spin singlet s -wave and spin-triplet chiral p -wave as in ref. [19]. The pairing matrix for the mix is

$$\hat{\Delta}(\mathbf{k}) = [\Delta_s \hat{\sigma}_0 + \Delta_p e^{i\theta} \hat{\sigma}_3] i\hat{\sigma}_2, \quad (3.10)$$

which is purely off-diagonal. Here Δ_s and Δ_p are the weights of the singlet and triplet parts. For each spin channel the pairing potential is related to both spin and direction of motion. For right-movers in the first (second) spin channel $\uparrow\downarrow$ ($\downarrow\uparrow$), the pairing potential felt by a moving quasiparticle is $\Delta_{\uparrow\downarrow}(\theta_+) = \Delta_s + \Delta_p e^{i\theta}$ [$\Delta_{\downarrow\uparrow}(\theta_+) = -(\Delta_s - \Delta_p e^{i\theta})$] and for left-movers $\Delta_{\uparrow\downarrow}(\theta_-) = \Delta_s - \Delta_p e^{-i\theta}$ [$\Delta_{\downarrow\uparrow}(\theta_-) = -(\Delta_s + \Delta_p e^{-i\theta})$]. Thus the singlet-triplet mix also gives rise to the appearance of two effective gaps $\Delta_1 = |\Delta_s + \Delta_p e^{i\theta}|$ and $\Delta_2 = |\Delta_s - \Delta_p e^{i\theta}|$, depending on the direction of motion.

3.6 Model for ferromagnet-superconductor hybrid junctions

We model ferromagnet-superconductor hybrid junctions as a ferromagnet-ferromagnetic insulator-superconductor (F-FI-S) junction. We assume a flat interface located at $x=0$. The ferromagnetic region is in $x < 0$ and the superconductor in $x > 0$. The effective mass m in both regions is assumed to be the same. For the ferromagnet, we adopt the Stoner model, for which the effect of the spin polarization can be described by an effective single particle Hamiltonian with an exchange energy h_0 . The ferromagnetic insulator for up (down) spin is described by a potential

$$V_{\uparrow(\downarrow)}(\mathbf{x}) = (V_0 \pm U_B)\delta(x), \quad (3.11)$$

where $\delta(x)$ is the delta function, V_0 is the barrier amplitude and U_B is the exchange amplitude. The spatial variation of the superconducting gap function $\Delta(\mathbf{k})$ is given by the superconducting coherence length ξ_0 . Assuming that ξ_0 is much larger than the Fermi coherence length (i.e., the Fermi energy is much larger than the superconducting energy gap, $E_F \gg \Delta$), we can neglect the decay of the gap function near the interface and ignore self-consistency. The gap function can now be written as

$$\Delta(\theta_S, T, x) = \Delta(\theta_S, T)\Theta(x), \quad (3.12)$$

where the spatial dependence is given by the step function $\Theta(x)$. The temperature dependence of the gap is given by the interpolation function

$$\Delta(\theta_S, T) = \Delta(\theta_S) \left(\tanh 1.74 \sqrt{T_c/T - 1} \right), \quad (3.13)$$

Where T_c is the critical temperature of the superconductor and T is temperature.

The BdG-equations for both up and down spin channels can now be written as

$$\begin{pmatrix} H_\sigma(x) & s_\sigma \Delta_\sigma(\theta_S, T) \Theta(x) \\ s_\sigma \Delta_\sigma^*(\theta_S, T) \Theta(x) & -H_\sigma(x) \end{pmatrix} \begin{pmatrix} u_\sigma \\ v_\sigma \end{pmatrix} = \varepsilon \begin{pmatrix} u_\sigma \\ v_\sigma \end{pmatrix}, \quad (3.14)$$

where

$$H_\sigma(x) = H_0(x) \mp h_0 \Theta(-x) + v_\sigma(x) \quad (3.15)$$

with $\mp h_0$ for up and down spins. ε is the quasiparticle energy. In the ferromagnetic region, the wave vector is written as

$$k_{\uparrow(\downarrow)} = |\mathbf{k}_{\uparrow(\downarrow)}| = \sqrt{2m/\hbar^2 (E_{FN} + \varepsilon \pm h_0)}, \quad (3.16)$$

with E_{FN} as the Fermi energy in the ferromagnet. For wavevectors under the wideband or semiclassical approximation, $\varepsilon \ll E_{FN}$, and the wave vectors in the ferromagnet can be approximated as

$$k_{\uparrow(\downarrow)} \approx k_{FN} \sqrt{1 \pm X} \quad (3.17)$$

where k_{FN} is the Fermi wave vector and $X = h_0/E_{FN}$. We will refer to X as polarization. The number of up (down) spins is $N_\uparrow(N_\downarrow)$. The spin filtering of quasiparticles in the ferromagnet for up (down) spins are $P_{\uparrow(\downarrow)} = N_{\uparrow(\downarrow)}/(N_\uparrow + N_\downarrow) = (E_{FN} \pm h_0)/2E_{FN} = (1 \pm X)/2$.

Similarly, in the superconductor, as $\varepsilon, \Delta \ll E_{FS}$, with E_{FS} as the Fermi energy in the superconductor, the wave vectors $q_{e(h)}$ for the electron (ELQ) and hole-like (HLQ) quasiparticles can be written as

$$q_{e(h)} = |\mathbf{q}_{e(h)}| = \sqrt{2mE_{FS}/\hbar^2 \pm 2m\sqrt{\varepsilon^2 - |\Delta|^2}/\hbar^2} \approx \sqrt{2mE_{FS}/\hbar^2} = k_S. \quad (3.18)$$

As we are considering a junction with only one interface, our scattering problem is independent of the phase in the exponentials and the above approximation is justified. However, if one is dealing with multi-interface junctions or wishes to compute the pairing potential self-consistently, the phases must be included and the term $2m\sqrt{\varepsilon^2 - |\Delta|^2}/\hbar^2$ can't be ignored.

Ferromagnet FI Superconductor

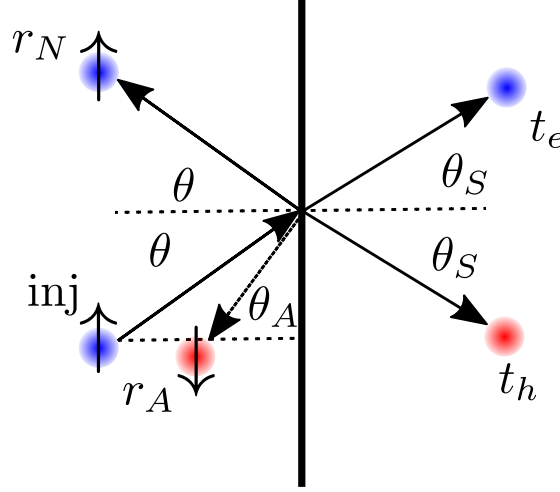


Figure 3.1: Scattering processes in F-FI-S junction. Assuming an up spin injection from the ferromagnet, the possible processes are normal reflection r_N , Andreev reflection r_A and transmissions of ELQ t_e and HLQ t_h . The Andreev reflected particle has an opposite spin to the injection and thus the injection angle θ is not equal to the angle of the Andreev reflected particle θ_A if $h_0 \neq 0$.

Assuming up-spin particle injection at an angle θ , measured with respect to the x-direction (perpendicular to the F-S interface), we have four possible processes; normal reflection r_N , Andreev reflection r_A , and transmission of ELQ t_e and HLQ t_h (figure 3.1). As we have chosen to study pairings for which the Cooper pair has opposite spins, the Andreev reflected particle has an opposite spin to the injection. Thus the injection angle θ is not equal to the angle of the Andreev reflected particle θ_A if $h_0 \neq 0$. As explained in section 3.2, we assume that the momentum is conserved in the y-direction. This yields an analog of Snell's law:

$$k_{\uparrow} \sin \theta = k_{\downarrow} \sin \theta_A = k_S \sin \theta_S, \quad (3.19)$$

which has several important implications, including the existence of critical angles, in analogy with well-known phenomena in optics. When the incident angle is $\theta > \sin^{-1}(k_S/k_{\uparrow}) = \theta_{cl}$, there are no real solutions to equation (3.19). The scattering problem does not have a solution with propagating wave vectors in the superconducting region and total reflection will occur. The probability of normal reflection $|r_e(\varepsilon, \theta)|^2 = 1$ and there is no current flow from the ferromagnet to the superconductor. When $k_{\downarrow} < k_s < k_{\uparrow}$, the

x-component of the wave vector of the Andreev reflection ($\sqrt{k_\downarrow^2 - k_s^2 \sin^2 \theta_S}$) becomes purely imaginary for $\theta > \sin^{-1}(k_\downarrow/k_\uparrow) = \theta_{c2}$. A propagating wave from an Andreev reflection is thus impossible and there is no current flowing from the ferromagnet to the superconductor. However, transmitted quasiparticles from the ferromagnet to the superconductor do propagate and result in a current. This evanescent Andreev reflection is usually referred to as virtual Andreev Reflection (VAR).

Assuming particle injection from the ferromagnet with spin up (down) and following the general solutions of the the BdG equations from section 3.1, the x-component of the wave function can be written as

$$\Psi_\sigma(x) = e^{ik_\sigma \cos \theta x} \begin{pmatrix} 1 \\ 0 \end{pmatrix} + r_{A,\sigma} e^{ik_{\tilde{\sigma}} \cos \theta_A x} \begin{pmatrix} 0 \\ 1 \end{pmatrix} + r_{N,\sigma} e^{-ik_\sigma \cos \theta x} \begin{pmatrix} 1 \\ 0 \end{pmatrix}, \quad (3.20)$$

for $x < 0$ in the ferromagnet with $\sigma = \uparrow, \downarrow$ and $\tilde{\sigma} = \downarrow, \uparrow$. For $x > 0$ in the superconductor

$$\Psi_\sigma(x) = t_{e,\sigma} e^{ik_S \cos \theta_S x} \begin{pmatrix} u_\sigma(\theta_+) \\ \eta_\sigma^*(\theta_+) v_\sigma^*(\theta_+) \end{pmatrix} + t_{h,\sigma} e^{-ik_S \cos \theta_S x} \begin{pmatrix} \eta_\sigma(\theta_-) v_\sigma(\theta_-) \\ u_\sigma(\theta_-) \end{pmatrix}. \quad (3.21)$$

Here we have adopted the definitions of gap phase $\eta_\sigma(\theta_\pm) = s_\sigma \Delta_\sigma(\theta_\pm, T) / |\Delta_\sigma(\theta_\pm, T)|$ and the angles $\theta_+ = \theta_S$ and $\theta_- = \pi - \theta_S$ to distinguish between right moving ELQ (t_e) and left moving HLQ (t_h). The reflection coefficients are obtained by matching the wave functions at the F-S interface, under the boundary conditions

$$\begin{aligned} \Psi_{x>0}|_{x=0} &= \Psi_{x<0}|_{x=0}, \\ (\partial_x \Psi_{x<0} - \partial_x \Psi_{x<0})|_{x=0} &= k_F S \begin{pmatrix} Z_{\uparrow(\downarrow)} & 0 \\ 0 & Z_{\downarrow(\uparrow)} \end{pmatrix} \Psi_{x<0}|_{x=0}, \end{aligned} \quad (3.22)$$

where $Z_{\uparrow(\downarrow)} = Z_0 \pm Z_m = 2m/\hbar^2(V_0 \pm U_B)$. From now on, we will refer to Z_m as the exchange amplitude to distinguish it from the exchange energy of the ferromagnet. For $\theta_{c1} < \theta$, we simply have $r_{N,\sigma} = 1$ and $r_{A,\sigma} = t_{e,\sigma} = t_{h,\sigma} = 0$ and the current vanishes. For $\theta < \theta_{c1}$, we have

$$\begin{aligned}
r_{e,\uparrow(\downarrow)} &= -[(1 - \lambda_{1,\uparrow(\downarrow)} - iZ'_{\uparrow(\downarrow)})(1 + \lambda_{2,\uparrow(\downarrow)} - iZ'_{\downarrow(\uparrow)}) \\
&\quad - (1 + \lambda_{1,\uparrow(\downarrow)} - iZ'_{\uparrow(\downarrow)})(1 - \lambda_{2,\uparrow(\downarrow)} + iZ'_{\downarrow(\uparrow)})\hat{\Gamma}_+\hat{\Gamma}_-]/\gamma, \\
r_{a,\uparrow(\downarrow)} &= \frac{4\lambda_{1,\uparrow(\downarrow)}\hat{\Gamma}_+}{\gamma}, \\
t_{e,\uparrow(\downarrow)} &= \frac{i2\lambda_{1,\uparrow(\downarrow)}(1 + \lambda_{2,\uparrow(\downarrow)} - iZ'_{\downarrow(\uparrow)})}{\gamma}, \\
t_{h,\uparrow(\downarrow)} &= \frac{-i2\lambda_{1,\uparrow(\downarrow)}\hat{\Gamma}_+(1 - \lambda_{2,\uparrow(\downarrow)} - iZ'_{\downarrow(\uparrow)})}{\gamma}, \\
\gamma &= (1 + \lambda_{1,\uparrow(\downarrow)} + iZ'_{\uparrow(\downarrow)})(1 + \lambda_{2,\uparrow(\downarrow)} - iZ'_{\downarrow(\uparrow)}) \\
&\quad - (1 - \lambda_{1,\uparrow(\downarrow)} - iZ'_{\uparrow(\downarrow)})(1 - \lambda_{2,\uparrow(\downarrow)} + iZ'_{\downarrow(\uparrow)})\hat{\Gamma}_+\hat{\Gamma}_-,
\end{aligned} \tag{3.23}$$

with

$$\begin{aligned}
Z'_{\uparrow(\downarrow)} &= \frac{Z_{\uparrow(\downarrow)}}{\cos\theta_S}, \quad \Gamma_{\pm} = \frac{\Delta_{\uparrow(\downarrow)}(\theta_{\pm})}{\varepsilon + \sqrt{\varepsilon^2 - |\Delta_{\uparrow(\downarrow)}(\theta_{\pm})|^2}}, \\
\lambda_{1,\uparrow(\downarrow)} &= \frac{k_{\uparrow(\downarrow)} \cos\theta}{k_S \cos\theta_S}, \quad \lambda_{2,\uparrow(\downarrow)} = \frac{k_{\downarrow(\uparrow)} \cos\theta_A}{k_S \cos\theta_S}.
\end{aligned} \tag{3.24}$$

For $\theta_{c2} < \theta < \theta_{c1}$, $\lambda_{2,\uparrow(\downarrow)}$ becomes imaginary due to the VAR process described earlier. Using the solved reflection amplitudes the spectral differential conductance $\hat{\sigma}_{\uparrow(\downarrow)}(\varepsilon, \theta)$ at zero temperature in the superconductor for the up and down spin injection channels is given by [10] [5]

$$\tilde{\sigma}_{\uparrow(\downarrow)}(\varepsilon, \theta) = \frac{2e^2}{h} \text{Re} \left[\left(1 + \frac{\lambda_{2,\uparrow(\downarrow)}}{\lambda_{1,\uparrow(\downarrow)}} |r_{a,\uparrow(\downarrow)}|^2 - |r_{e,\uparrow(\downarrow)}|^2 \right) \right]. \tag{3.25}$$

We take the real part of the above equation due to the fact that λ_2 can be imaginary when VAR process occurs. The normalized spectral conductance $\tilde{\sigma}_R$ for a particular injection angle is defined as

$$\tilde{\sigma}_R(\varepsilon, \theta) = \frac{\sigma_{\uparrow}(\varepsilon, \theta)P_{\uparrow} + \sigma_{\downarrow}P_{\downarrow}(\varepsilon, \theta)}{\hat{\sigma}_N(\theta)}, \tag{3.26}$$

where the normal ($\Delta = 0$) conductance for F-FI-N junction is

$$\tilde{\sigma}_N = \frac{2e^2}{h} (\tilde{\sigma}_{N,\uparrow}(\theta)P_{\uparrow} + \tilde{\sigma}_{N,\downarrow}(\theta)P_{\downarrow}), \tag{3.27}$$

with

$$\tilde{\sigma}_{N,\uparrow(\downarrow)}(\theta) = \frac{4\lambda_{1,\uparrow(\downarrow)}}{|1 + \lambda_{1,\uparrow(\downarrow)} + iZ'_{\uparrow(\downarrow)}|^2}. \quad (3.28)$$

The normalized conductance $\sigma(\varepsilon)$ is obtained by an angle-average of $\tilde{\sigma}_{\uparrow(\downarrow)}(\varepsilon, \theta)$

$$\sigma(\varepsilon) = \frac{1}{\sigma_N} \int_{-\frac{\pi}{2}}^{\frac{\pi}{2}} d\theta \cos \theta [(\tilde{\sigma}_{\uparrow}(\varepsilon, \theta)P_{\uparrow}k_{\uparrow}) + (\tilde{\sigma}_{\downarrow}(\varepsilon, \theta)P_{\downarrow}k_{N,\downarrow})], \quad (3.29)$$

with normal conductance

$$\sigma_N = \frac{2e^2}{h} \int_{-\frac{\pi}{2}}^{\frac{\pi}{2}} d\theta \cos \theta [(\tilde{\sigma}_{N,\uparrow}(\theta)P_{\uparrow}k_{\uparrow}) + (\tilde{\sigma}_{N,\downarrow}(\theta)P_{\downarrow}k_{\downarrow})]. \quad (3.30)$$

The current through the junction is

$$I(eV, T, \delta T) = \int_{-\infty}^{\infty} d\varepsilon [f(\varepsilon - eV, T + \delta T) - f(\varepsilon, T)] \int_{-\frac{\pi}{2}}^{\frac{\pi}{2}} d\theta \cos \theta [(\tilde{\sigma}_{\uparrow}(\varepsilon, \theta)P_{\uparrow}k_{\uparrow}) + (\tilde{\sigma}_{\downarrow}(\varepsilon, \theta)P_{\downarrow}k_{N,\downarrow})] \quad (3.31)$$

where eV is the applied bias voltage in the ferromagnet, T is reference temperature in the superconductor, δT is the temperature gradient applied in the ferromagnetic side and

$$f(\varepsilon, T + \delta T) - f(\varepsilon, T) = (1 + e^{\frac{\varepsilon - eV}{T + \delta T}})^{-1} - (1 + e^{\frac{\varepsilon}{T}})^{-1} \quad (3.32)$$

is the difference between the Fermi functions in the ferromagnet and the superconductor. From the current, if we set the temperature gradient to 0, the differential conductance at finite temperature T for a voltage bias eV is

$$\frac{dI(eV, T, \delta T = 0)}{dV} = \int_{-\infty}^{\infty} \sigma(\varepsilon) \frac{d}{dV} [f(\varepsilon - eV, T) - f(\varepsilon, T)] d\varepsilon. \quad (3.33)$$

We will only consider thermoelectric currents, the currents created by a temperature bias δT , without a voltage bias eV . By setting $eV = 0$ the difference between the Fermi functions $f(\varepsilon, T + \delta T) - f(\varepsilon, T)$ in equation 3.31 is now an asymmetric function, which is shown in figure 3.2 for $T = 0.03\Delta_0$ and different values of the temperature bias, $\delta T = 0.03\Delta_0$, $0.1\Delta_0$ and $0.3\Delta_0$. Here we have expressed the temperature T and the gradient δT in units of the energy gap Δ_0 , keeping in mind that the relation between the critical temperature T_c and the energy gap at zero temperature is [20]

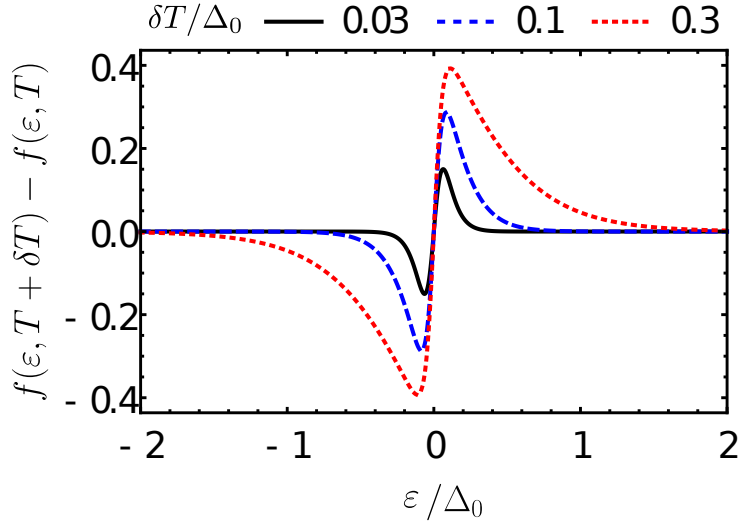


Figure 3.2: Difference between Fermi functions from equation (3.32) in the F and S regions for different values of the temperature gradient δT . We set $T = 0.03\Delta_0$ and $eV = 0$.

$$\frac{\Delta_0}{T_c} = 1.764. \quad (3.34)$$

The temperature is thus $T = 0.03\Delta_0 \approx 0.05T_c$, $T = 0.3\Delta_0 \approx 0.5T_c$ and so on. When only a temperature bias is applied, the difference between the Fermi functions is always antisymmetric. Thus in order to see a finite current for δT , the conductance $\sigma(\varepsilon)$ needs to be asymmetric as well.

Chapter 4 Results

4.1 N-I-S junction

We will first consider a normal metal-insulator-superconductor (N-I-S) junction. For simplicity, we will assume the Fermi level of the metal and the superconductor to be the same, so $E_{FN} = E_{FS} = E_F$. Setting the exchange energy of the ferromagnet $h_0 = 0$ and the exchange amplitude $Z_m = 0$, so that $Z_\uparrow = Z_\downarrow = Z_0$, we can solve the scattering amplitudes for the N-I-S junction from the solutions of eq.(3.23). We consider six different pairing potentials from the table 3.1 and will refer to these pairings as pure pairings. We will also discuss the singlet-triplet mix of the pairing potential introduced in section 3.5. The barrier amplitude $Z_0 = 5$ is the same for all discussed cases, representing a strong barrier in the tunneling limit.

The normalized conductance spectra $\hat{\sigma}_R$ and the corresponding total normalized angular averaged conductance σ are depicted for the six different pure potentials in figures 4.1 and 4.2. In the conductance spectra the color of the spectra represents the magnitude of the normalized conductance, with brighter areas corresponding to a larger conductance. The vertical axis is the quasiparticle energy ε normalized by the gap amplitude Δ_0 and the horizontal axis is the injection angle θ . As the transverse component of the momentum can be parametrized by the angle θ , the spectra corresponds to the dispersion relation. In the upper row we collect the gapful pairings s -wave, chiral d - and chiral p -wave. In the lower row the nodal pairings $d_{x^2-y^2}$ -, d_{xy} - and p_x -wave. For the gapful pairings the gap is constant for all values of the angle θ but for the nodal pairings the gap vanishes for certain θ values.

From the gapped superconductors the s -wave is trivial and the chiral ones are non-trivial, as they have subgap SAS. For the chiral pairings the subgap states have a large asymmetric angular dependence with respect to the inversion of the angle θ . This is a manifestation of the broken time reversal symmetry. We can also distinguish the $d_{x^2-y^2}$ -wave pairing as a trivial nodal one, as it has no subgap states, and d_{xy} - and p_x -wave as non-trivial nodal pairings. Non-trivial nodal pairings have flat zero-energy SAS formed for all θ . We can make one more classification with the zero bias peaks (ZBP) of

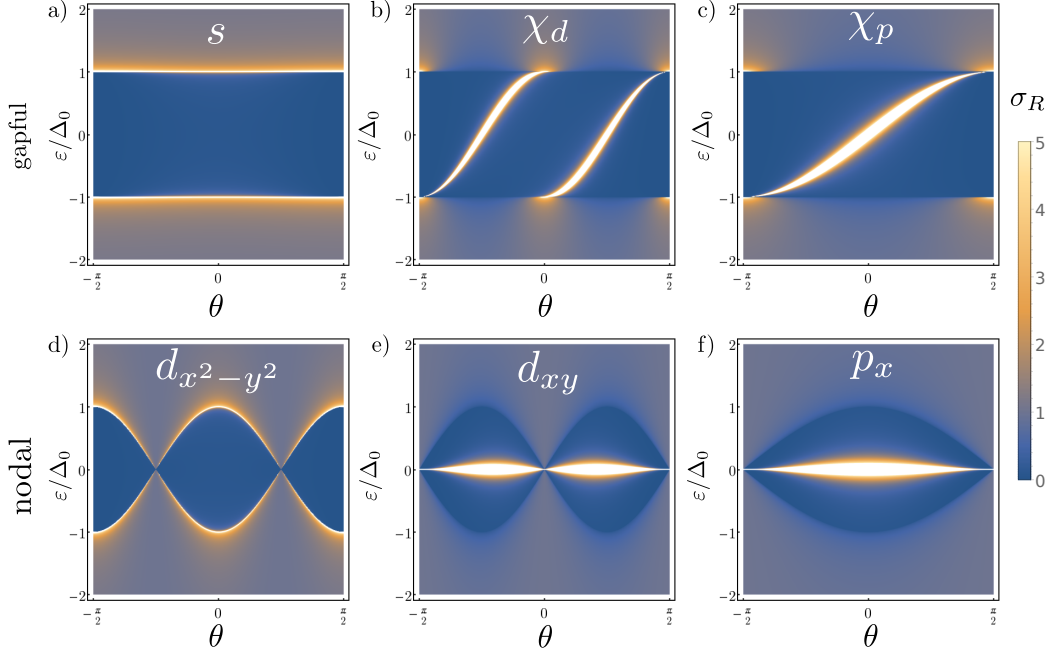


Figure 4.1: Normalized conductance spectra σ_R for six different pairing potentials in NIS junction with the barrier strength $Z_0=5$, a) s -wave, b) $d_{x^2-y^2}$ -wave, c) d_{xy} -wave, d) chiral p -wave, e) chiral d -wave and f) p_x -wave. In the upper row all the pairings are gapful, nodal in the bottom row. The color of the spectra represents the magnitude of the normalized conductance, the vertical axis is the quasiparticle energy ε normalized by the gap amplitude Δ_0 and the horizontal axis is the injection angle θ .

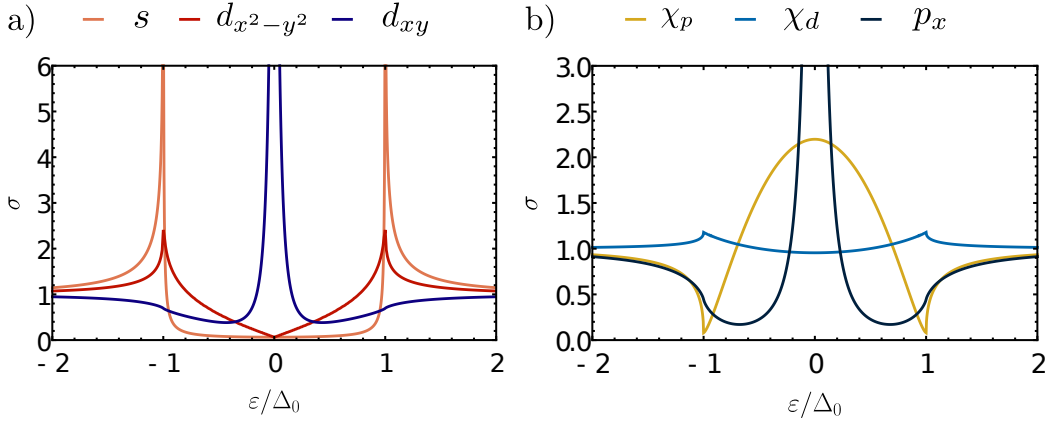


Figure 4.2: Total normalized angular averaged conductance σ for the different pairing potentials a) s -wave, $d_{x^2-y^2}$ -wave, d_{xy} -wave, b) chiral d - and p -wave and p_x -wave. These correspond to the cases in figure 4.1.

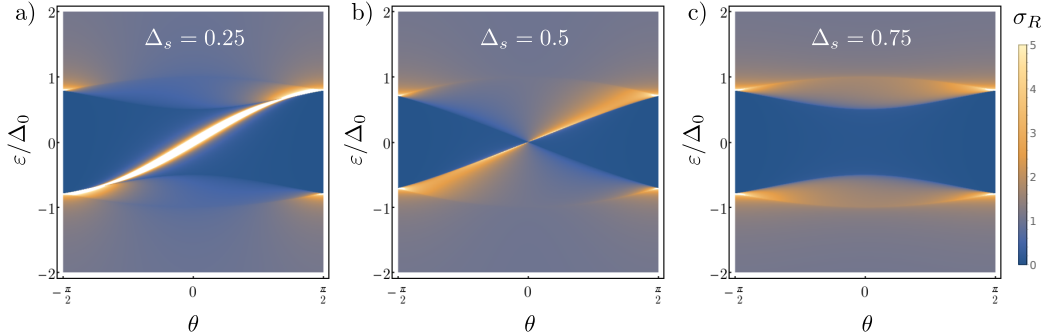


Figure 4.3: Normalized conductance spectra σ_R for the singlet-triplet mix with a) $\Delta_s < \Delta_p$ b) $\Delta_s = \Delta_p$ and c) $\Delta_s > \Delta_p$. The $\Delta_s = \Delta_p$ case is the quantum critical point, where the bulk gap has been closed, but the condition for the formation of the zero bias peak is not yet fulfilled.

the pairings in the angular averaged conductances in figure 4.2. The SAS of chiral p -wave result in a heavily broadened zero bias peak in the total conductance, but for the chiral d -wave the SAS do not result in a ZBP. Both d_{xy} - and p_x -wave exhibit a strong zero-bias peak due to the perfect Andreev reflections for all θ values at zero energy.

We also study the singlet-triplet mix for the NIS junction. Similarly to above, we show the conductance spectra and the corresponding total conductance in figures 4.3 and 4.4 for three different cases depending on the relative values of the singlet and triplet parts of the mix. Here $\Delta_s + \Delta_p = 1$. When Δ_s is close to 0, the triplet part of the mix dominates, and the singlet part dominates as we get closer to the value $\Delta_s = 1$.

From the spectra we can see that for all the cases the gap is no longer isotropic with respect to the angle θ , in contrast to the the pure s -wave and chiral p -wave pairings. This is the result of the interplay between the two effective gaps Δ_1 and Δ_2 . When $\Delta_s < \Delta_p$, the triplet part of the mixing dominates, and, consequently, the chiral p -wave subgap states appear in the conductance spectra. These states then contribute to the ZBP in the total conductance. For the singlet dominated case $\Delta_s \geq \Delta_p$, the conductance is suppressed for energies smaller than the effective gap Δ_2 , resembling the conventional s -wave case. In the intermediate region $\Delta_2 < |\epsilon| < \Delta_1$ the conductance slowly increases. When $\Delta_s = \Delta_p$ the gap closes at zero energy and zero angle. The spectra is asymmetric with respect to θ , but the zero bias peak is not yet formed, as can be seen from the total conductance. The

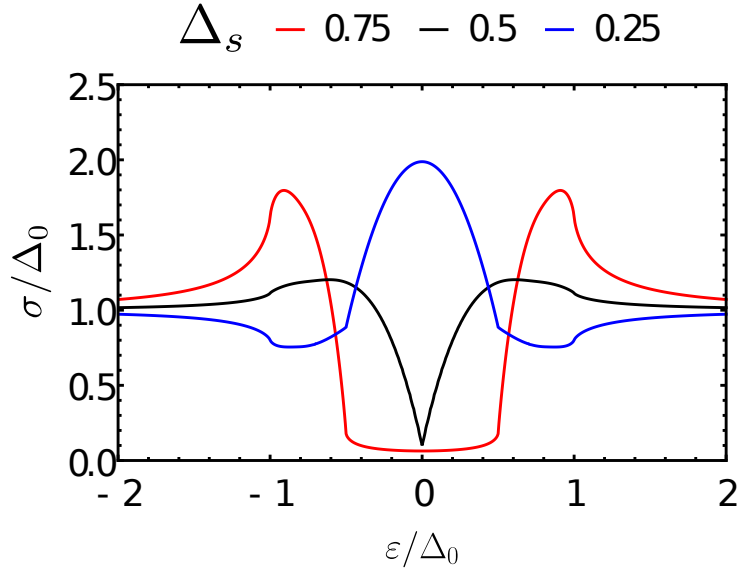


Figure 4.4: Normalized conductance σ corresponding to the three cases of figure 4.3 for the singlet-triplet mix.

$\Delta_s = \Delta_p$ is the quantum critical point that distinguishes the trivial phase dominated by the singlet from the non-trivial phase dominated by the triplet.

The impact of the two effective gaps Δ_1 and Δ_2 is further visualized in figure 4.5. We plot the conductance σ together with the contributions from the normal reflection $1 - |r_N|^2$ and the Andreev $(\lambda_2/\lambda_1)|r_A|^2$ for the corresponding cases in figures 4.3 and 4.4. When $|\varepsilon| < \Delta_2$, we are in the fully gapped region. The normal and Andreev part of the contributions are the same, as no other scattering processes than normal and Andreev reflection are allowed. In the intermediate region $\Delta_2 < |\varepsilon| < \Delta_1$ more scattering processes are allowed, as the particles subjected to Δ_2 are not in the gapped region anymore and we have a finite probability for quasiparticle transport to the superconductor. Due to this, the normal and Andreev part of the contributions start to deviate from each other and the Andreev reflections are heavily suppressed. For the case $\Delta_s = \Delta_p$, Δ_2 is fully closed, and for all energies $|\varepsilon| < \Delta_1$ all the scattering processes are allowed.

To summarize, we can classify the pure pairings with respect to their two-dimensional topological classification and examine the formation of the zero bias peak. In the singlet-triplet mix we can distinguish between two different phases, the trivial and non-trivial with a critical point separating them. In

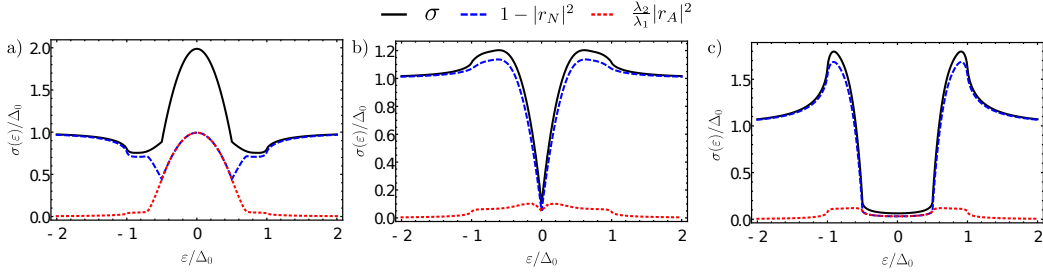


Figure 4.5: Normalized conductance σ with the normal $1 - |r_N|^2$ and Andreev $\text{Re}(\lambda_2/\lambda_1)|r_A|^2$ contributions corresponding to the three cases of figure 4.3 and 4.4 for the singlet-triplet mix: a) $\Delta_s = 0.25$ b) $\Delta_s = 0.25$ and c) $\Delta_s = 0.25$.

addition, the two effective gaps, Δ_1 and Δ_2 , of the singlet-triplet mix have a large effect on the transport processes.

4.2 Ferromagnet-Superconductor hybrid junctions

In this section we will consider the ferromagnet-superconductor hybrid junctions. First we will discuss independently the effects of the polarization X and the barrier exchange amplitude Z_m and then their combined effect for the pure pairings. For $X = 1$, we reach the half-metallic limit of full spin polarization and only the up spin channel contributes to the conductance. Depending on the parameters X or Z_m , which we will turn on/off, we will have different types of heterostructures; N-I-S junction when $X = 0$ and $Z_m = 0$, which we discussed last section; F-I-S when $X \neq 0$ and $Z_m = 0$; N-FI-S when $X = 0$ and $Z_m \neq 0$ and F-FI-S when $X \neq 0$ and $Z_m \neq 0$. We show the conductance spectra σ_R in figure 4.6 and the total conductance σ in figure 4.7 for the d_{xy} -wave pairing potential for all types of junctions. We chose the d_{xy} -wave in order to show the different effects clearly.

When we have a finite polarization $X = 0.5$ without the exchange amplitude (F-I-S case) the effect of the ZBP of the d_{xy} -wave pairing is reduced in the total conductance as can be seen from the red line of figure 4.7, when compared against the N-I-S conductance (gray line). With a finite polarization an injected particle with an up spin can go through a total reflection for critical angles θ_{c1} and virtual Andreev reflection for the critical angle θ_{c2} , as explained in Section 3.6. The effect of the critical angles is evident from the spectra of figure 4.6. For angles larger than θ_{c1} , the effect of the zero bias peak is reduced for the other spin channel, for our example here, with

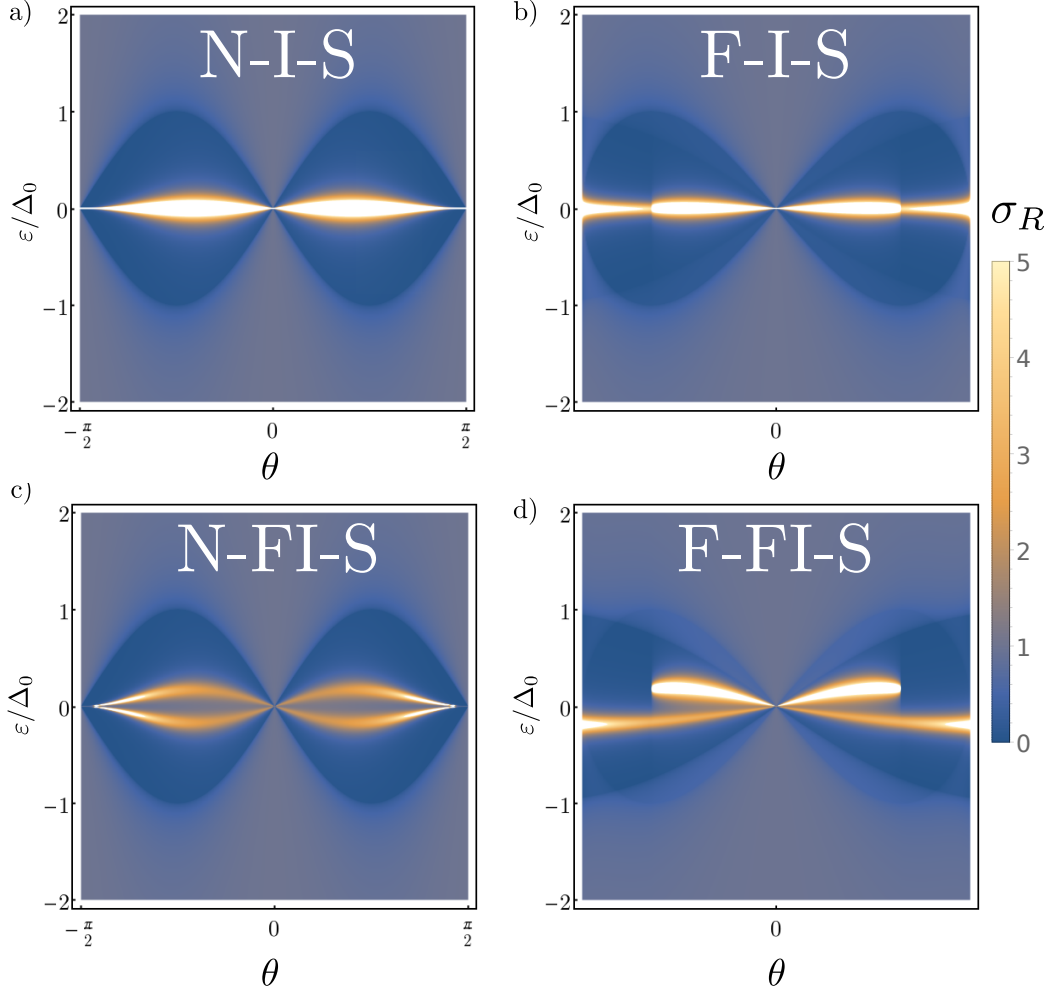


Figure 4.6: Normalized conductance spectra σ_R for d_{xy} -wave pairing in a) N-I-S, b) F-I-S, c) N-FI-S and d) F-FI-S junctions. We set $Z_0 = 5$, $X = 0.5$ and $Z_m = 2.5$.

$X = 0.5$, $\theta_{c1} \approx 55^\circ$. The effect of the polarization is also shown as the change in the shape of the gap in the spectra of figure 4.6, which is different for each spin channels. It can be seen, that for the injection with spin up, the gap is fully open at $\theta = \pi/2$, for which the other spin channel has a node in the gap, as in the N-I-S junction.

The effect of the exchange amplitude Z_m when $X = 0$ is shown in figure 4.6c and in the black line of figure 4.7. We have chosen $Z_m = 2.5$ so that $Z_\uparrow = 7.5$ and $Z_\downarrow = 2.5$. The conductance is shifted for higher (lower) energies for up (down) spins. This induces a spin splitting of the ZBP, which is clearly shown in both the conductance spectra and the total conductance.

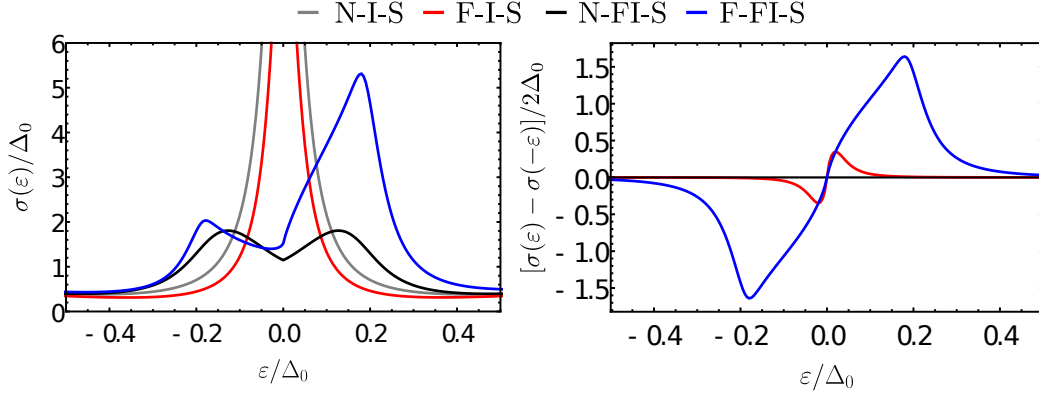


Figure 4.7: a) Normalized conductance σ and b) the asymmetric part of the total conductance $[\sigma(\epsilon) - \sigma(-\epsilon)]/2$ for d_{xy} -wave pairing corresponding to the cases of figure 4.6.

The combined effect of X and Z_m (thus the full F-FI-S junction) is shown in figure 4.6d with the integrated total conductance as the blue line of figure 4.7a. We choose the same values for X and Z_m as above. As for the N-FI-S junction, the exchange amplitude Z_m induces a spin splitting of the ZBP and the polarization X weakens the states due to the total reflection and VAR process. For the up spin channel the splitted peak is thus cut of for angles smaller than θ_{c1} . This combined effect of the spin splitting and the polarization leads to an asymmetry with respect to the zero energy. We can thus expect a thermoelectric effect.

At first look, it might seem that only the combined effect of Z_m and X would produce an asymmetry with respect to zero energy by looking at the conductance spectra in figure 4.6 and the total conductance in figure 4.7. However, when plotting the asymmetric part of the conductance $[\sigma(\epsilon) - \sigma(-\epsilon)]/2$, shown in figure 4.7b, we see that also the polarization X only (F-I-S junction, red line) is enough to create asymmetry, although the effect is noticeably weaker than for the F-FI-S junction (blue line). The polarization alone is thus enough to create asymmetry, but the spin splitting induced by Z_m enhances it.

The asymmetry in the total conductance leads to a thermoelectric current, as it is shown in figure 4.8 for both the full F-FI-S junction ($X = 0.5$ and $Z_m = 2.5$) in the upper row and the polarized F-I-S junction ($X = 0.5$, $Z_m=0$) in the lower row. We plot the thermoelectric currents for all the pairings considered in Section 4.1. When computing the currents, the base

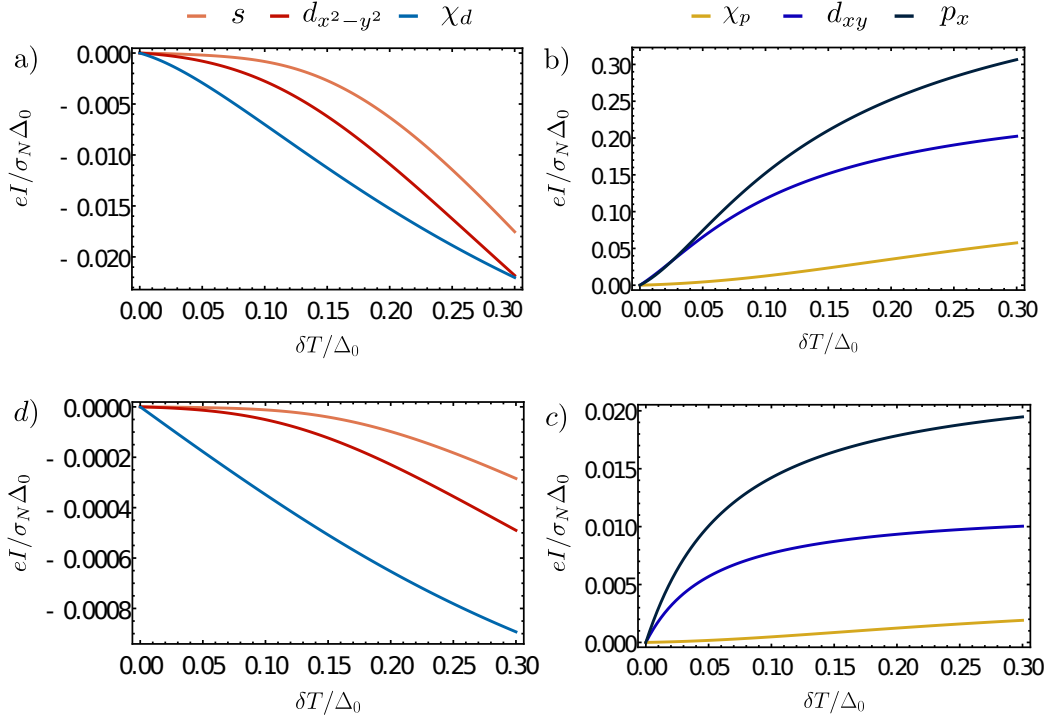


Figure 4.8: Thermoelectric current I at $T = 0.03\Delta_0$ for a), c) s -, $d_{x^2-y^2}$ - and chiral d -wave b), d) d_{xy} -, chiral p - and p_x -wave. In the upper row we have F-FI-S junction with $X = 0.5$ and $Z_m = 2.5$ and in the lower row F-I-S where $X = 0.5$ and $Z_m = 0$. For both we set $Z_0 = 5$.

temperature of the superconductor is set at $T = 0.03\Delta_0$, which is approximately $0.05T_c$. The temperature gradient δT is also measured as a function of Δ_0 , ranging from 0 to $0.3\Delta_0$. We are only interested in the effect of the temperature bias, so the voltage bias is $eV = 0$.

Qualitatively, the behaviour is similar for both junctions, but the value of the current for the N-FI-S junction is significantly weaker. As with the asymmetric part of the conductance, the polarization is enough to create a thermoelectric current with the exchange amplitude Z_m increasing it. We also see a different behaviour with respect to the pairing potential. For all the pairing potentials having a ZBP, d_{xy} -, chiral p - and p_x -wave the thermoelectric current is positive. The strength of the current also follows the strength of the zero bias peak, p_x -wave being the highest and chiral p -wave the weakest. For the pairings without a ZBP, s -, $d_{x^2-y^2}$ - and chiral d -wave the current is negative. Chiral d -wave has the largest negative current, due to its subgap SAS.

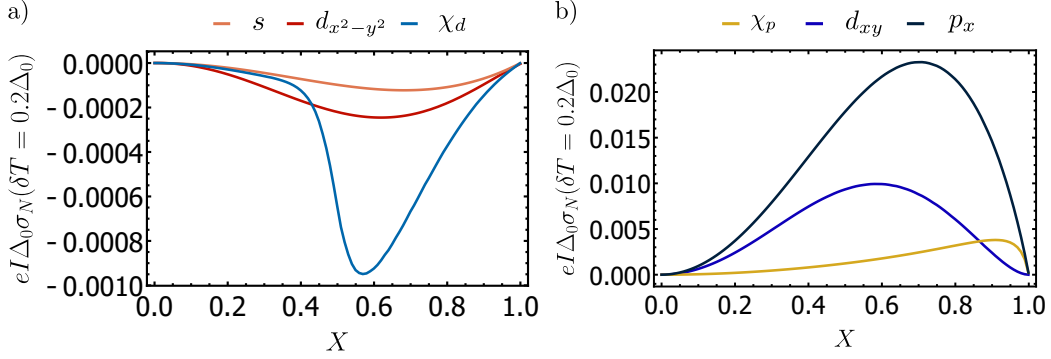


Figure 4.9: Thermoelectric current I at $T = 0.03\Delta_0$ and $\delta T = 0.2\Delta_0$ as a function of polarization X for a) s -, $d_{x^2-y^2}$ - and chiral d -wave b) d_{xy} -, chiral p - and p_x -wave in the F-I-S junction where $Z_m = 0$ and $Z_0 = 5$.

The effect of the polarization X for different pairing potentials can be seen in figure 4.9, where the thermoelectric current is plotted at $T = 0.03\Delta$ and $\delta T = 0.2\Delta$. Here, we only discuss the effect of X and set $Z_m = 0$, so the barrier strength for each spin species is the same. We see the same behaviour with respect to the pairings as in figure 4.8. For the zero bias peaked pairings the thermoelectric current is positive, for others it is negative. Also the value of the current follows the strength of the ZBP (figure 4.9). We see that there is an optimal value of polarization, for which the current is at its maximum strength, which is different for each pairing. For all the pairings a maximum polarization is reached for large polarization values ($X > 0.5$), but when approaching the half-metallic limit ($X = 1$) the thermoelectric current vanishes. When we approach the half-metallic limit, only one of the spin channels affects the current, and we no longer break the particle-hole symmetry between the spin species, the requirement for a thermoelectric effect. Also, with increasing X , both critical angles θ_{c1} and θ_{c2} increase, leading to high rates of total reflection and VAR, thus decreasing the current.

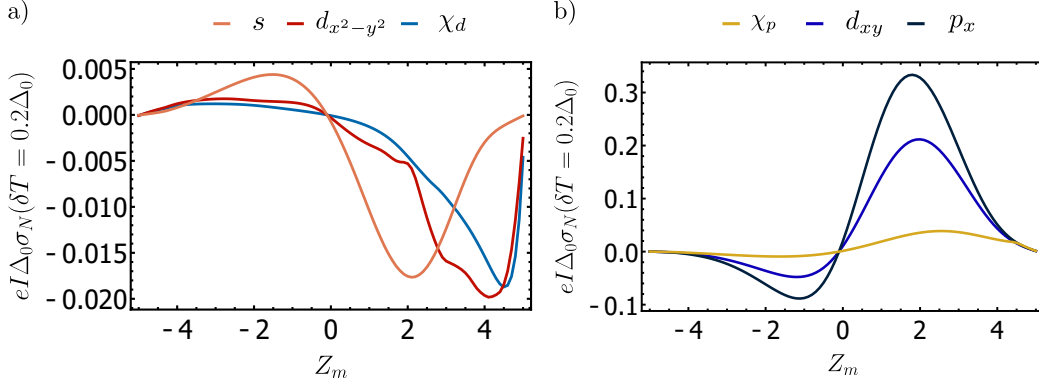


Figure 4.10: Thermoelectric current I at $T = 0.03\Delta_0$ and $\delta T = 0.2\Delta_0$ as a function of exchange amplitude Z_m for a) s -, $d_{x^2-y^2}$ - and chiral d -wave b) d_{xy} -, chiral p - and p_x -wave in the F-I-S junction where $X = 0.5$ and $Z_0 = 5$.

The thermoelectric current can be created with only the spin polarization X , but combining it with the spin splitting effect of the exchange amplitude Z_m , we can increase the current. We plot the thermoelectric current as a function of Z_m for $X = 0.5$, $T = 0.03\Delta$ and $\delta T = 0.2$ in figure 4.10. Here, we set $X = 0.5$ since the spin splitting effect of Z_m was not enough to create asymmetry in the conductance, and, consequently, a thermoelectric current. In figure 4.10 we vary Z_m from -5 to 5. when $Z_m = \pm 5$ we have that $Z_{\uparrow(\downarrow)} = 10$ and $Z_{\downarrow(\uparrow)} = 0$, so for the up (down) spin particle the junction is in the tunnel regime and for the down (up) spin particle the junction is at the transparent regime. For $Z_m = 0$, we have $Z_{\uparrow} = Z_{\downarrow}$, and no asymmetry.

All the pairings present a sign change at $Z_m = 0$. For the pairings with a ZBP we have a negative current for negative values of Z_m and vice versa. The sign of the current follows the previously noticed pattern. The sign of the current is opposite between the pairings with a ZBP and the pairings without a ZBP. There is an optimal value for Z_m , but as with X , it differs from pairing to pairing, especially for the non-ZBP pairings. For positive Z_m values the current is stronger for all cases. The polarization X created positive thermoelectric currents for the ZBP pairings, negative for non-ZBP pairings. The positive Z_m enhances the effect of X , and negative values compete against it. Z_m increases the current up to an order of magnitude when comparing with the values of figure 4.9. At the points where $Z_m = \pm 5, 0$, the current does not disappear fully, but it is an order of magnitude smaller, as only the effect of the polarization X remains.

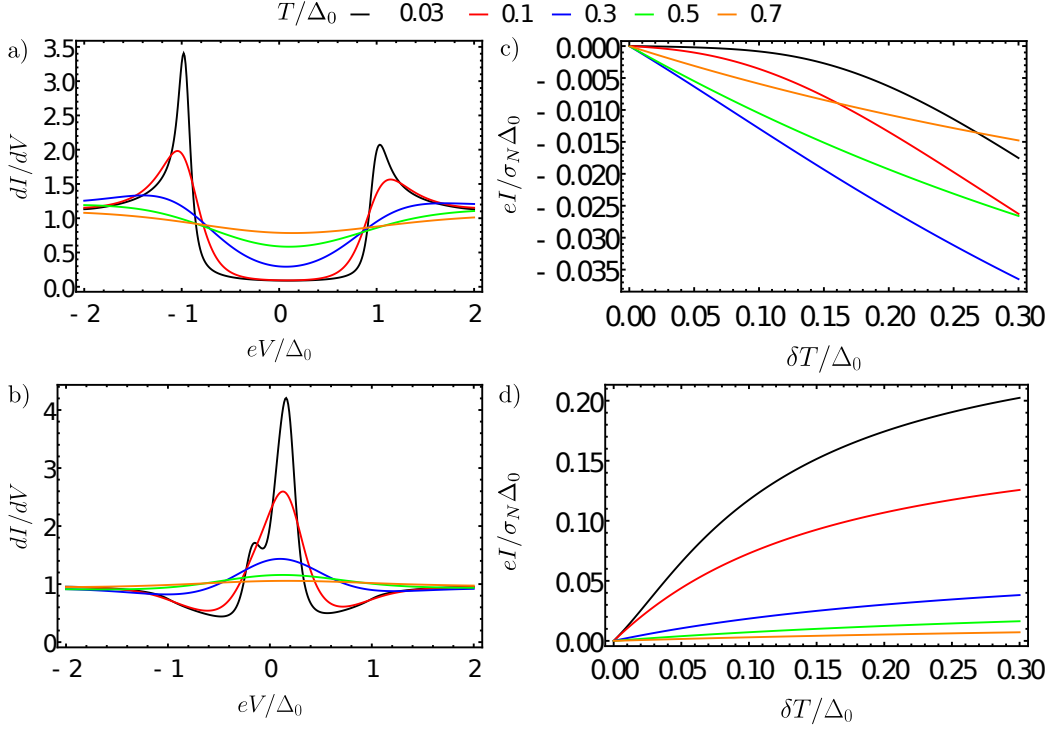


Figure 4.11: Differential conductance at finite temperature dI/dV and thermoelectric current I for a), b) s -wave and c), d) d_{xy} -wave. Here $X = 0.5$ and $Z_m = 2.5$.

4.2.1 Temperature effects

Finally, we discuss the effect of temperature. In figure 4.11 we show the differential conductance at finite temperature dI/dV and the corresponding thermoelectric current for s -wave and d_{xy} -wave. Here we have set $X = 0.5$ and $Z_m = 2.5$ for a F-FI-S junction. Increasing the temperature flattens out the conductance spectrum and the variation with respect to the normal state conductance decreases. The asymmetry is thus more difficult to notice. However, a finite thermoelectric current can still be observed, as shown in figures 4.11b and d. The sign of the thermoelectric current does not change with increasing temperature, but its value decreases.

With temperature gradient we can thus distinguish between the different pairings at high temperatures, even if the corresponding differential conductance becomes hard to distinguish. We also notice a difference in behaviour between the s -wave and d_{xy} -wave in the current. For the s -wave, the current increases with temperature until a maximum is reached ($T = 0.3\Delta_0$, blue

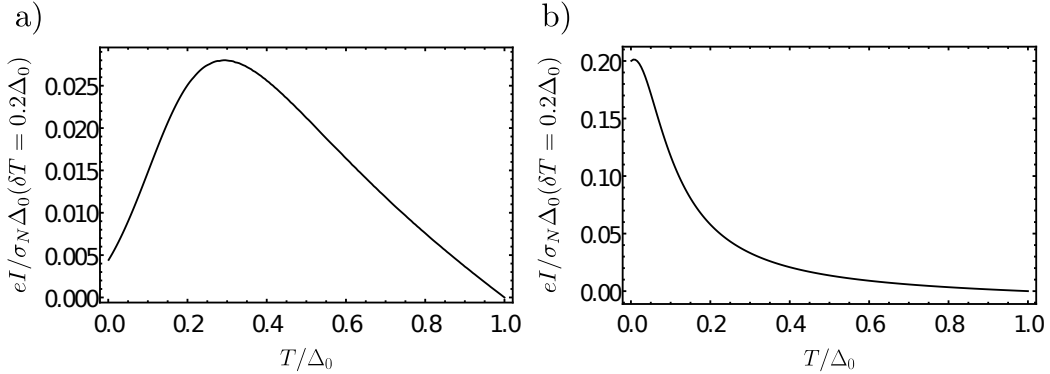


Figure 4.12: Thermoelectric current I at $\delta T = 0.2\Delta_0$ as a function of temperature T for a) s -wave and b) d_{xy} -wave. We set $X = 0.5$ and $Z_m = 2.5$.

line in figure 4.11b), and then its value starts to decrease towards zero with increasing temperature. For the d_{xy} -wave the temperature increase leads to a monotonical decrease in the current. This is further verified in figure 4.12, where we have the current at $\delta T = 0.2\Delta_0$ for both pairings, corresponding to the cases in figure 4.11. S -wave has maximum at $T = 0.3\Delta_0$ and d_{xy} -wave has a maximum almost at the zero temperature, after which it monotonically decreases.

4.3 Singlet-triplet mix in F-S junctions

The behaviour of the thermoelectric current I at $T = 0.03\Delta_0$ and $\delta T = 0.2\Delta_0$ for the singlet-triplet mix is plotted in figure 4.13 for F-I-S ($X = 0.5$ and $Z_m = 0$), N-FI-S ($X = 0$ and $Z_m = 2.5$) and F-FI-S ($X = 0.5$ and $Z_m = 2.5$) junctions as a function of the amplitude of the singlet part of the mix Δ_s with $\Delta_p = 1 - \Delta_s$. When Δ_s is close to 0, the triplet part of the mix dominates, and the singlet part dominates as we get closer to the value $\Delta_s = 1$. We immediately notice a difference when comparing to the pure pairings discussed in the previous section. For the pure pairings, in the N-FI-S junction the exchange amplitude Z_m did not create asymmetry in the conductance, and, consequently, was not enough to create the thermoelectric current without the polarization X . For the mix we see that a finite current is created for the N-FI-S junction, with values of the same order of magnitude as for the F-FI-S junction. The F-I-S junction with only the polarization X results also in a thermoelectric current, but its values are an order of magnitude lower than for the N-FI-S and F-FI-S junctions. For the singlet-triplet mix, we can see a thermoelectric effect with polarization X , exchange amplitude Z_m and

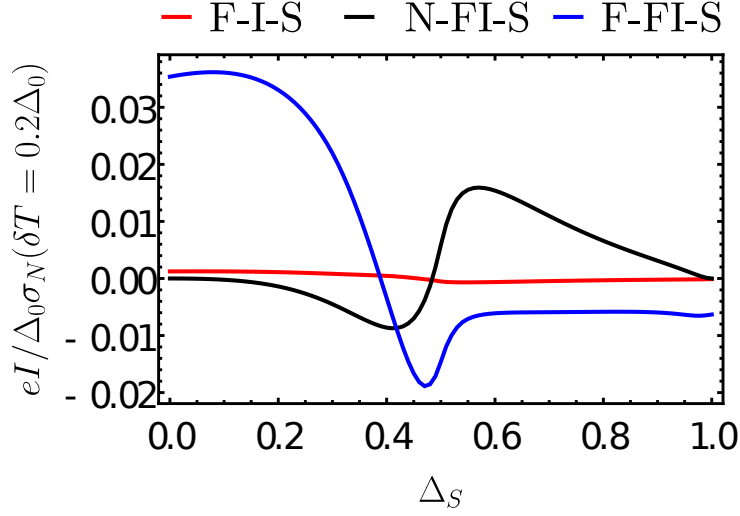


Figure 4.13: Thermoelectric current I normalized with the normal conductance σ_N at $\delta T = 0.2\Delta_0$ for the singlet-triplet mix in F-I-S ($X = 0.5$ and $Z_m = 0$), N-FI-S ($X = 0$ and $Z_m = 2.5$) and F-FI-S ($X = 0.5$ and $Z_m = 2.5$) junctions. We set $Z_0 = 5$ and $T = 0.03\Delta_0$ and vary the amplitude of the singlet part Δ_s of the mix.

their combination.

For all the cases in figure 4.13, the current changes sign. However, this sign change does not occur at the same value of Δ_s , yet it is in the vicinity of the point $\Delta_s = 0.5$, where the phase transition from topologically trivial region to a non-trivial one occurred in the N-I-S junction. The F-I-S junction follows the behaviour of the pure pairings. When we are on the triplet dominated region $\Delta_s < \Delta_p$, the current is positive. When the singlet dominates, $\Delta_s > \Delta_p$, the current is negative. In the triplet dominating region, $\Delta_s < 0.5$, the F-FI-S junction behaves qualitatively as the pure chiral p case. The thermoelectric current is positive in the F-I-S junction, and it is enhanced by Z_m in the F-FI-S junction. When moving to the intermediate region, close to point $\Delta_s = \Delta_p = 0.5$, the sign of the current changes from positive to negative, with a minimum in the vicinity of the point $\Delta_s = 0.5$. When the singlet dominates, $\Delta_s > 0.5$, the current reaches a saturation point. In the N-FI-S junction we see that as we approach the intermediate region, the current is enhanced. Interestingly, the sign of the current has been reversed when comparing to all the other previously discussed cases. In the triplet dominated region it is negative, and changes to positive as the weight of the singlet part is increased. In the pure limit, $\Delta_s = 0, 1$, the current is 0, as expected.

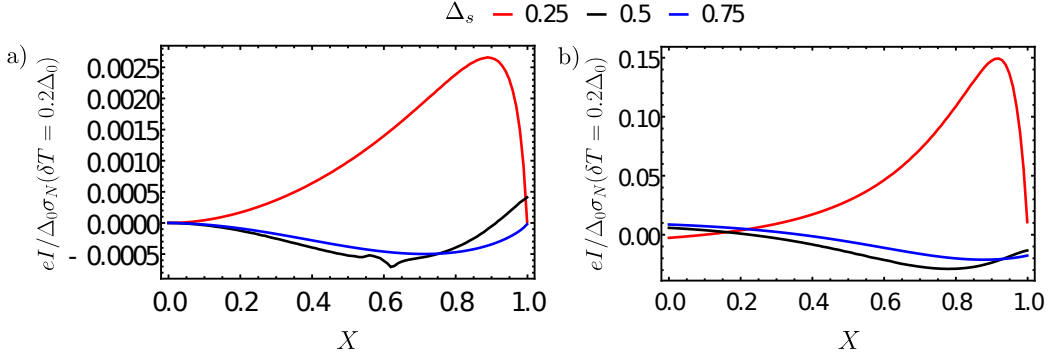


Figure 4.14: Thermoelectric current I normalized with the normal conductance σ_N at $\delta T = 0.2\Delta_0$ as a function of X for the a) F-I-S ($Z_m = 0$) and b) F-FI-S ($Z_m = 2.5$) junctions. We set $Z_0 = 5$ and $T = 0.03\Delta_0$.

In figure 4.14 we vary the polarization X for F-I-S and N-FI-S junctions. As before, the value of the current is larger for the F-FI-S, as the exchange amplitude Z_m enhances the current. When comparing with the values for the pure pairings, the enhancing is now stronger. The values in the F-FI-S junction are two orders of magnitude larger than in the F-I-S junction. The triplet dominated region ($\Delta_s = 0.25$, red line) behaves similarly to the pure chiral p case. Increasing polarization increases the current, with a maximum around the value $X \approx 0.9$, and tends to 0 when approaching the half-metallic limit. In the F-I-S junction (figure 4.14a) the current is zero at $X = 0$ and the half-metallic limit. In the F-FI-S (figure 4.14b) the current does not go to zero at these limits as the exchange amplitude Z_m is enough to create a thermoelectric effect. This can also be seen for the singlet dominated case ($\Delta_s = 0.75$, blue line) and the intermediate case ($\Delta_s = 0.5$, black line). The singlet dominated case behaves qualitatively as the pure s -wave pairing. For the intermediate case we see an interesting effect in the F-I-S junction. When approaching the half-metallic limit, the current does not vanish, but changes sign from negative to positive.

The thermoelectric current is plotted as a function of Z_m for N-FI-S and F-FI-S junctions in figure 4.15. The values of the current are the same order of magnitude for both junctions. We notice that the values of the current are not as high, as was for the pure cases. However, the current behaves differently in the N-FI-S junction than we have seen before. As we vary Z_m the sign of the current does not change as for the F-FI-S junction. Also, the sign of the current for the singlet dominated and the intermediate mix

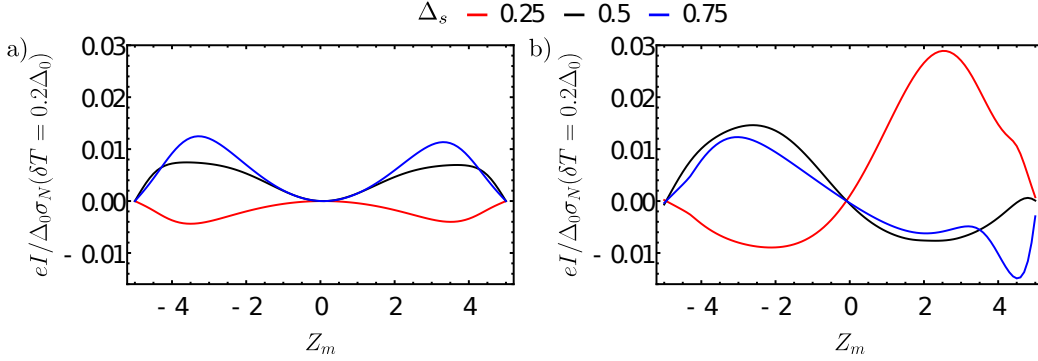


Figure 4.15: Thermoelectric current I normalized with the normal conductance σ_N at $\delta T = 0.2\Delta_0$ as a function of Z_m for the a) N-FI-S ($X = 0$ and $Z_m = 2.5$) and b) F-FI-S ($X = 0.5$ and $Z_m = 2.5$) junctions. We set $Z_0 = 5$ and $T = 0.03\Delta_0$.

is positive, and for the triplet dominated mix negative. There is also an asymmetry with the negative and positive Z_m values. For positive Z_m values $Z_\uparrow > Z_\downarrow$ and vice versa. At the points $Z_m = 0$ and $Z_m = \pm 5$ the current vanishes. The F-FI-S junction behaves similarly to the pure cases discussed in the previous section. The sign of the current is negative for the triplet dominated region for negative Z_m values and the current becomes positive for positive Z_m values.

The exchange amplitude Z_m is enough to create a thermoelectric effect for the singlet-triplet mix in F-S junctions. We enlighten this in figure 4.16. We plot the normalized conductance $\sigma(\varepsilon)$ (black lines) from equation (3.29) and the separated contribution from the normal processes $1 - |r_N|^2$ (blue lines) and the Andreev reflections $(\lambda_2/\lambda_1)|r_A|^2$ (red lines) in the N-FI-S junctions with $Z_m = 2.5$ and $Z_0 = 5$ in the first column. In the second column we have the anti-symmetric part of the conductance $[\sigma(\varepsilon) - \sigma(-\varepsilon)]/2$ and similarly for the normal and Andreev contributions. We plot these for different values of the singlet amplitude of the mix, from top-down: $\Delta_s = 0.25, 0.5, 0.75$. As discussed in Section 4.1, in the intermediate region $\Delta_2 < |\varepsilon| < \Delta_1$ we can have quasiparticle transport to the superconductor. In this intermediate region, the spin splitting effect of Z_m leads to asymmetry, and, consequently, to thermoelectric current as we have shown. In the fully gapped region $|\varepsilon| < \Delta_1$ the splitting is not enough to create asymmetry, as is shown for $\Delta_s = 0.25$ and $\Delta_s = 0.75$ in figure 4.16. For $\Delta_s = \Delta_p$ the gap Δ_2 closes, and for all energies $|\varepsilon| < \Delta_1$ all the scattering processes are possible, and conductance is fully asymmetric inside the gap Δ_1 . Andreev processes are heavily sup-

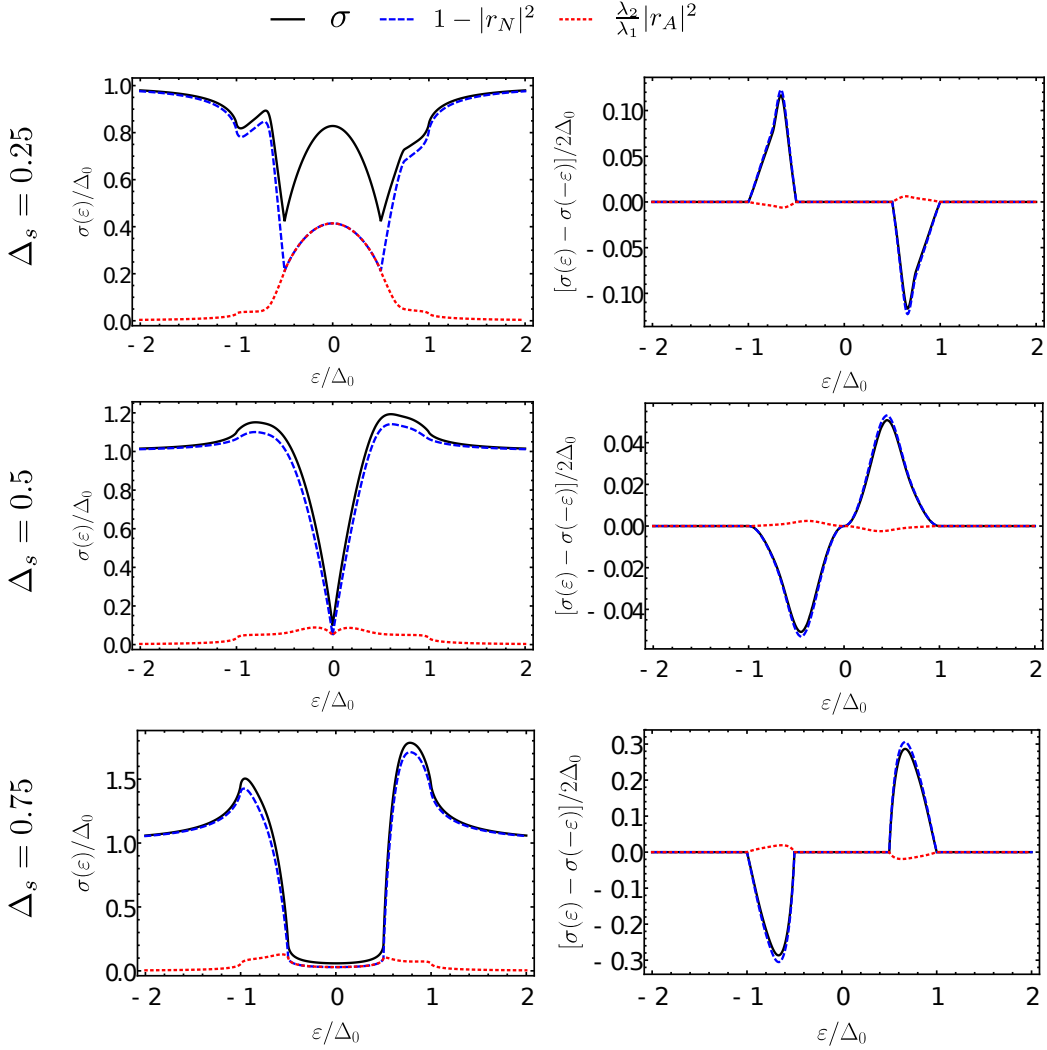


Figure 4.16: Normalized conductance $\sigma(\varepsilon)$ (left column) and its asymmetric $[\sigma(\varepsilon) - \sigma(-\varepsilon)]/2$ part (right column) plotted for different values of the singlet amplitude Δ_s . First row: $\Delta_s = 0.25$, second row $\Delta_s = 0.5$ and third row $\Delta_s = 0.75$. We set $X = 0$, and $Z_m = 2.5$ with $Z_0 = 5$ for N-FI-S junction.

pressed in the intermediate region, and this is also apparent when inspecting the anti-symmetric part. In the N-FI-S junction with singlet-triplet mix pairing, the thermoelectric effect is mostly due to the quasiparticle transport to the superconductor.

We plot the conductance and normal and Andreev contributions for F-FI-S junction in figure 4.17, setting $X = 0.5$ in addition to N-FI-S junction in figure 4.16. We notice differences with respect to the N-FI-S junction. The con-

ductance is now asymmetric for all energies $|\varepsilon| < \Delta_1$. Also, the sign on of the asymmetric part has been reversed. When $|\varepsilon| < \Delta_2$, the normal and Andreev contributions are equal, as before. For the pure triplet chiral p -wave, $\Delta_s = 0$, the contributions from the normal $1 - |r_N|^2$ and Andreev $(\lambda_2/\lambda_1)|r_A|^2$ part to the conductance are equal inside the gap. As we keep increasing the singlet amplitude Δ_s , the contributions start to deviate from each other. However, differing from the N-FI-S, in the intermediate region $\Delta_2 < |\varepsilon| < \Delta_1$ both the Andreev processes and quasiparticle transport have now a significant contribution to asymmetry. In the F-FI-S junction with singlet-triplet mix pairing both the Andreev processes and quasiparticle transport contribute to the thermoelectric effect.

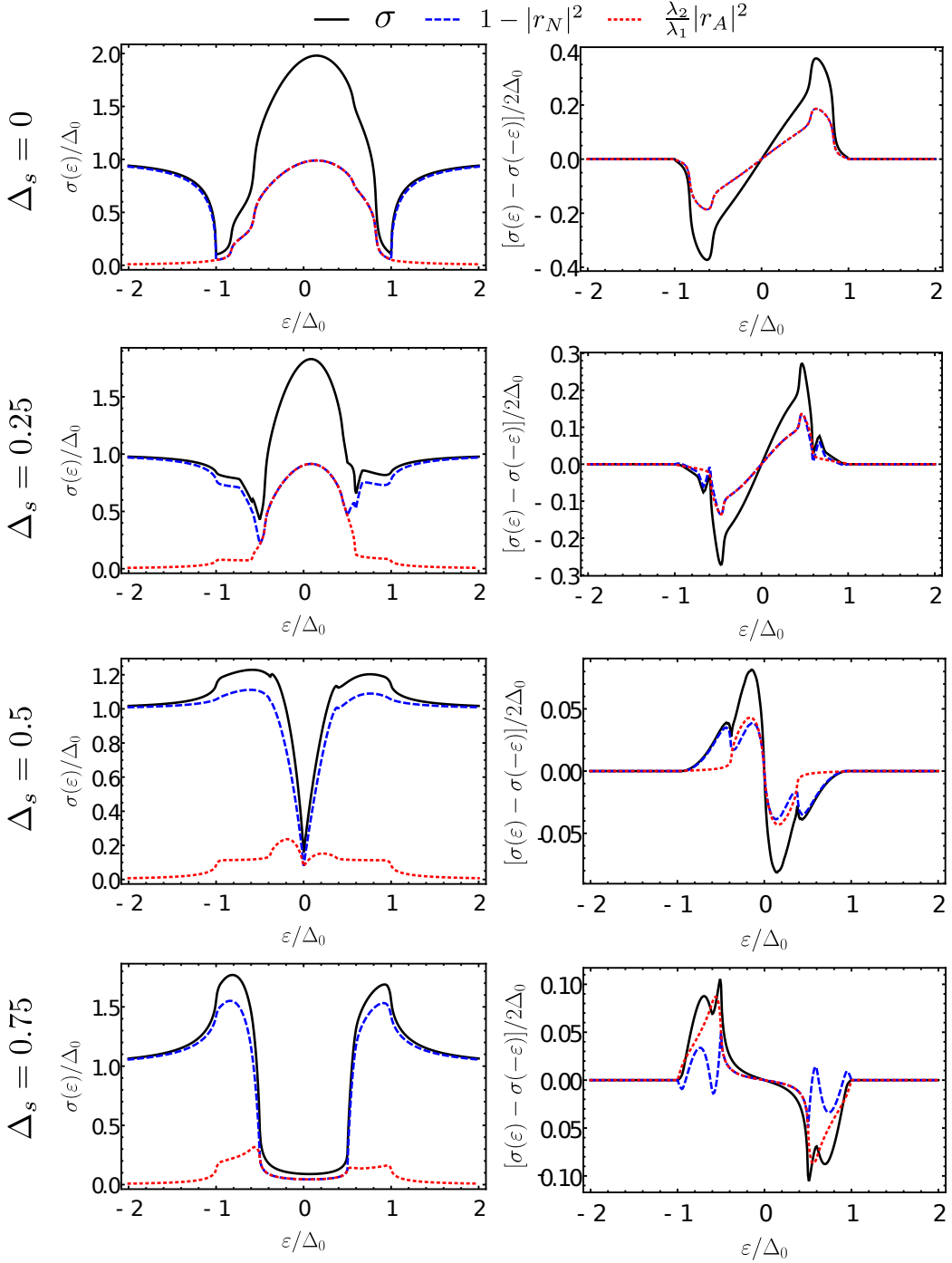


Figure 4.17: Normalized conductance $\sigma(\varepsilon)$ (left column) and its anti-symmetric $[\sigma(\varepsilon) - \sigma(-\varepsilon)]/2$ part (right column) plotted for different values of the singlet amplitude Δ_s . First row: $\Delta_s = 0$, second row $\Delta_s = 0.25$, third row $\Delta_s = 0.5$ and fourth row $\Delta_s = 0.75$. We set $X = 0.5$ and $Z_m = 2.5$ with $Z_0 = 5$ for F-FI-S junction.

Chapter 5 Conclusions

We have studied thermoelectric effects in ferromagnet-superconductor hybrid junctions. We used the approach of the scattering Bogoliubov-de Gennes formalism and the generalized BTK formula.

First, we studied the properties of different superconductors with the normal metal - insulator - superconductor (N-I-S) junction. Six different pairing potential symmetries were considered; the gapful symmetries s -, chiral d - and chiral p -wave and the nodal symmetries $d_{x^2-y^2}$ -, d_{xy} - and p_x -wave. We could classify these pure symmetries with respect to their two-dimensional topological classification (trivial and non-trivial with respect to the appearance of subgap surface Andreev states) and examine the formation of the zero bias peak. The latter proved to be an useful additional classification when considering thermoelectric effects.

We also discussed singlet-triplet mix of a trivial gapful s -wave symmetry and non-trivial chiral p -wave symmetry. In the singlet-triplet mix we could distinguish between two different phases, the trivial and non-trivial. The point $\Delta_s = \Delta_p$, where the weight of the singlet and triplet part of the mix is the same, is the critical point, where a phase change from trivial to non-trivial regime occurs. The singlet-triplet mix also gave rise to the appearance of two effective gaps. The two effective gaps, Δ_1 and Δ_2 , had a large effect on the transport processes. In the intermediate region $\Delta_2 < |\varepsilon| < \Delta_1$, in addition to the normal and Andreev reflections, quasiparticle transport to the superconductor is possible.

We discussed the conditions for a thermoelectric effect in the ferromagnet-superconductor junctions. For pure pairings, in order to have a thermoelectric current we need the spin polarization (X) in the ferromagnet-insulator-superconductor junction. The exchange amplitude Z_m in the ferromagnet-ferromagnetic insulator-superconductor junction enhances the effect via spin splitting.

The sign of the thermoelectric current depended on whether the pairing potential had a zero bias peak in its conductance spectrum. By varying Z_m we can enhance this effect and also change the sign of the current, but the

current of all pairings with a zero bias peak will have the same sign and vice versa. The effect of X is larger for the pairings with a zero bias peak, and the value of the effect follows the strength of the zero bias peak seen in the tunneling conductance. We found that there is an optimal polarization X and exchange amplitude Z_m value, different for each pairing.

For the singlet-triplet pairing a thermoelectric effect could be produced with polarization X and the exchange amplitude Z_m alone. The thermoelectric effect from Z_m in the N-FI-S junction was observed to occur from the spin splitting in the intermediate region $\Delta_2 < |\varepsilon| < \Delta_1$ and the current was mostly carried by a quasiparticle transport to the superconductor. In the F-FI-S junction both Andreev and quasiparticle processes contributed to the thermoelectric effect.

Our results here show that the symmetry of superconducting pairing potential has a significant effect in the thermoelectric effects observed in superconducting hybrid junctions. The utilized methodology can be further extended and as an outlook we give straightforward ideas for exploring the results presented here further. A possible continuation of the current work is to consider three-dimensional superconductors, where we can further complicate the properties of the pairing potential. Other future extension should be a detailed study on the optimal values of the polarization X and the exchange amplitude Z_m and their contributions to the thermoelectric figures of merit. One could also use the solutions presented here in order to solve the Green's function of the considered systems, and through it connect the thermoelectric current to the total induced pairing.

Bibliography

- [1] J. Bardeen, L. N. Cooper, and J. R. Schrieffer. “Theory of Superconductivity”. In: *Phys. Rev.* 108 (5 Dec. 1957), pp. 1175–1204. DOI: 10.1103/PhysRev.108.1175. URL: <https://link.aps.org/doi/10.1103/PhysRev.108.1175>.
- [2] Leon N. Cooper. “Bound Electron Pairs in a Degenerate Fermi Gas”. In: *Phys. Rev.* 104 (4 Nov. 1956), pp. 1189–1190. DOI: 10.1103/PhysRev.104.1189. URL: <https://link.aps.org/doi/10.1103/PhysRev.104.1189>.
- [3] J. G. Bednorz and K. A. Müller. “Possible high T_c superconductivity in the Ba-La-Cu-O system”. In: *Zeitschrift für Physik B Condensed Matter* 64 (June 1986), pp. 189–193. DOI: 10.1007/BF01303701.
- [4] Manfred Sigrist and Kazuo Ueda. “Phenomenological theory of unconventional superconductivity”. In: *Rev. Mod. Phys.* 63 (2 Apr. 1991), pp. 239–311. DOI: 10.1103/RevModPhys.63.239. URL: <https://link.aps.org/doi/10.1103/RevModPhys.63.239>.
- [5] Satoshi Kashiwaya and Yukio Tanaka. “Tunnelling effects on surface bound states in unconventional superconductors”. In: *Reports on Progress in Physics* 63.10 (2000), p. 1641. URL: <http://stacks.iop.org/0034-4885/63/i=10/a=202>.
- [6] C.W.J. Beenakker. “Search for Majorana Fermions in Superconductors”. In: *Annual Review of Condensed Matter Physics* 4.1 (2013), pp. 113–136. DOI: 10.1146/annurev-conmatphys-030212-184337. eprint: <https://doi.org/10.1146/annurev-conmatphys-030212-184337>. URL: <https://doi.org/10.1146/annurev-conmatphys-030212-184337>.
- [7] Pablo Burset et al. “Current fluctuations in unconventional superconductor junctions with impurity scattering”. In: *Phys. Rev. B* 95 (22 June 2017), p. 224502. DOI: 10.1103/PhysRevB.95.224502. URL: <https://link.aps.org/doi/10.1103/PhysRevB.95.224502>.
- [8] N. W. Ashcroft and N. D. Mermin. *Solid State Physics*. Holt-Saunders, 1976.

- [9] F. Sebastian Bergeret et al. “Colloquium: Nonequilibrium effects in superconductors with a spin-splitting field”. In: *Rev. Mod. Phys.* 90 (4 Oct. 2018), p. 041001. DOI: 10.1103/RevModPhys.90.041001. URL: <https://link.aps.org/doi/10.1103/RevModPhys.90.041001>.
- [10] G. E. Blonder, M. Tinkham, and T. M. Klapwijk. “Transition from metallic to tunneling regimes in superconducting microconstrictions: Excess current, charge imbalance, and supercurrent conversion”. In: *Phys. Rev. B* 25 (7 Apr. 1982), pp. 4515–4532. DOI: 10.1103/PhysRevB.25.4515. URL: <https://link.aps.org/doi/10.1103/PhysRevB.25.4515>.
- [11] Yukio Tanaka and Satoshi Kashiwaya. “Theory of Tunneling Spectroscopy of d -Wave Superconductors”. In: *Phys. Rev. Lett.* 74 (17 Apr. 1995), pp. 3451–3454. DOI: 10.1103/PhysRevLett.74.3451. URL: <https://link.aps.org/doi/10.1103/PhysRevLett.74.3451>.
- [12] Satoshi Kashiwaya et al. “Theory for tunneling spectroscopy of anisotropic superconductors”. In: *Phys. Rev. B* 53 (5 Feb. 1996), pp. 2667–2676. DOI: 10.1103/PhysRevB.53.2667. URL: <https://link.aps.org/doi/10.1103/PhysRevB.53.2667>.
- [13] M. J. M. de Jong and C. W. J. Beenakker. “Andreev Reflection in Ferromagnet-Superconductor Junctions”. In: *Physical Review Letters* 74.9 (Feb. 1995), pp. 1657–1660. ISSN: 1079-7114. DOI: 10.1103/physrevlett.74.1657. URL: <http://dx.doi.org/10.1103/PhysRevLett.74.1657>.
- [14] S. Kashiwaya et al. “Spin current in ferromagnet-insulator-superconductor junctions”. In: *Phys. Rev. B* 60 (5 Aug. 1999), pp. 3572–3580. DOI: 10.1103/PhysRevB.60.3572. URL: <https://link.aps.org/doi/10.1103/PhysRevB.60.3572>.
- [15] A. F. Andreev. “Thermal conductivity of the intermediate state of superconductors”. In: *Sov. Phys. JETP*. 19.5 (1964), p. 1228. URL: <http://www.jetp.ac.ru/cgi-bin/e/index?a=s&auid=124717>.
- [16] T. M. Klapwijk. “Proximity Effect From an Andreev Perspective”. In: *Journal of Superconductivity* 17.5 (Oct. 2004), pp. 593–611. ISSN: 1572-9605. DOI: 10.1007/s10948-004-0773-0. URL: <https://doi.org/10.1007/s10948-004-0773-0>.
- [17] Chr. Bruder. “Andreev scattering in anisotropic superconductors”. In: *Phys. Rev. B* 41 (7 Mar. 1990), pp. 4017–4032. DOI: 10.1103/PhysRevB.41.4017. URL: <https://link.aps.org/doi/10.1103/PhysRevB.41.4017>.

- [18] P. A. Frigeri et al. “Superconductivity without Inversion Symmetry: MnSi versus CePt₃Si”. In: *Phys. Rev. Lett.* 92 (9 Mar. 2004), p. 097001. DOI: 10.1103/PhysRevLett.92.097001. URL: <https://link.aps.org/doi/10.1103/PhysRevLett.92.097001>.
- [19] Pablo Burset et al. “Transport signatures of superconducting hybrids with mixed singlet and chiral triplet states”. In: *Phys. Rev. B* 90 (8 Aug. 2014), p. 085438. DOI: 10.1103/PhysRevB.90.085438. URL: <https://link.aps.org/doi/10.1103/PhysRevB.90.085438>.
- [20] Michael Tinkham. *Introduction to Superconductivity*. 2nd ed. Dover Publications, June 2004. ISBN: 0486435032. URL: <http://www.worldcat.org/isbn/0486435032>.